

Arctic regional changes revealed by clustering of sea-ice observations

Amélie Simon¹², Pierre Tandeo¹³, Florian Sévellec²³,
Camille Lique²

¹ IMT Atlantique, Lab-STICC, UMR CNRS 6285, 29238, Brest, France

² Univ Brest CNRS Ifremer IRD, Laboratoire d'Océanographie Physique et Spatiale (LOPS), Brest, France

³ ODYSSEY Team-Project, INRIA CNRS, Brest, France

35 Abstract

36
37 Understanding the evolution of Arctic sea-ice is crucial due to its climatic and
38 socio-economic impacts. Usual descriptors (e.g., sea-ice extent, sea-ice age, and
39 ice-free duration) quantify changes but do not account for the full seasonal cycle.
40 Here, using satellite observations of sea-ice concentration (SIC) over 1979-2023, we
41 perform a k-means clustering of the Arctic sea-ice seasonal cycle, initializing with
42 equal quantile separation and using Mahalanobis distance. Without providing prior
43 information, this data-driven method shows that the Arctic is best described by four
44 types of seasonal cycles: open-ocean (no ice year-round), permanent sea-ice (full
45 coverage with a minimum of 70% SIC), and two clusters showing ice-free conditions
46 ($SIC < 0.15$), namely partial and full winter freezing. The latter has larger SIC in winter,
47 more abrupt melting and freezing periods, and a shorter ice-free season than the
48 former. This reduction of dimension in the data suggests that the first date of retreat
49 is a good indicator for ice-free conditions the following summer and the first date of
50 advance a good indicator for fully ice cover conditions the following winter. The
51 pan-Arctic probability to belong to the permanent sea-ice seasonal cycle has
52 decreased by 3.1 %/decade which is compensated with an increase of probability to
53 belong to the open-ocean cluster (1.6 % per decade), the full winter freezing cluster
54 (1.1 % per decade) and the partial winter-freezing cluster (0.5 % per decade).
55 Regionally, the permanent sea-ice retraction from the Pacific side is compensated by
56 the full winter-freezing cluster while the open-ocean cluster expansion in the Atlantic
57 side is lost by the partial winter-freezing cluster. From the Beaufort to the Kara Seas,
58 the southern parts have stabilized (experiencing a new typical seasonal cycle,
59 corresponding to the full winter-freezing cluster) and the northern part have
60 destabilized (losing their typical permanent sea-ice seasonal cycle). Therefore, this
61 work provides a new way to describe Arctic regional changes using a statistical
62 framework based on physical behaviours of sea-ice and calls for a more latitudinal
63 vision of the Arctic regions.

64

65 Short summary

66 This work determines regions in the Arctic having common ice behaviours
67 throughout the year. Our research shows that, over the last four decades, a transition
68 has occurred in the Pacific side of the Arctic from ice all year round to seasonal ice
69 having an abrupt melting and growth phase. This transition has occurred closer and
70 closer to the pole by about 3% every decade. On the Atlantic side, the open ocean
71 has replaced seasonal ice having a smooth melting and growth phase.

72

73 Keywords

74 Arctic sea-ice, seasonal cycle, machine learning, clustering, climate change, satellite
75 dataset, regionalization

76

77

78 Introduction

79

80 The Arctic region has experienced rapid changes over recent decades that are
81 expected to intensify in the future (Shu et al., 2022). For a global warming of 1°C, the
82 Arctic has warmed by about 2.5 °C. In a 4°C warmer world, the Arctic is projected to
83 be from 7°C to 10°C warmer (IPCC, 2021; their Figure SPM.5). One of the main
84 mechanisms behind this Arctic amplification is the retreat of sea-ice, giving way to an
85 open-ocean that captures more solar radiation, an effect called surface albedo
86 feedback (Pithan and Mauritsen, 2014; Goosse et al., 2018). The observed Arctic
87 sea-ice loss has been attributed to human influence primarily because of greenhouse
88 gas emissions dominated by carbon dioxide and methane (Eyring et al., 2021 in IPCC,
89 their section 3.4.1.1).

90 The decline of the Arctic sea-ice has profound implications for the regional
91 environment and for almost four million people living beyond the Arctic circle.
92 Reduced ice cover increases light availability, which can enhance phytoplankton
93 blooms (Vancoppenolle et al., 2013). This, in turn, reshapes the food web structure

94 (Ardyna and Arrigo, 2020) and has significant consequences for fisheries, potentially
95 impacting catch levels and spatial distribution (Stock et al., 2017). The formation and
96 melting of sea ice also largely influences nearly all aspects of life for marine mammals
97 in the Arctic. A delay in winter sea-ice formation can trigger marine mammals'
98 unusual mortality events, as it has been the case in 2018 in the Bering Sea (Siddon et
99 al., 2020). Indigenous hunting opportunities that are dependent on the presence of
100 sea-ice have decreased and shifted in time (Huntington et al., 2017). Besides, new
101 ice-free regions could open industrial shipping routes and offshore oil and gas
102 exploration with associated risks of oil spills, marine mammal strikes and noise
103 pollution and lead to tension between nations (Galley et al., 2013; Huntington et al.,
104 2020).

105 The sea-ice retreat not only affects the Arctic locally but also plays a pivotal
106 role in the global Earth's radiative budget (Forster et al., 2021 in IPCC, their section
107 7.4.2.3) and a potential role in the modulation of remote large-scale oceanic and
108 atmospheric circulation, known as Arctic teleconnections (Deser et al., 2015; Cohen
109 et al., 2020; Simon et al., 2021; Smith et al., 2022). Therefore, describing the
110 evolution of the Arctic sea ice on a dynamic basis is important due to its fast
111 evolution, which has implications for both local and global climate and
112 socio-economic systems.

113 Different methods have been classically used in the literature to describe the
114 recent changes in Arctic sea-ice. Most of them are based on the analysis of sea-ice
115 concentration (SIC), which is obtained from satellite measurements since 1979 over
116 the full Arctic region. In comparison, observational datasets of sea-ice thickness are
117 available only for less than two decades and are still associated with large
118 uncertainties (Ricker et al. 2017). The sea-ice area (SIA; integral sum of the product of
119 SIC and area of all grid cells) or the sea-ice extent (SIE; integral sum of the areas of all
120 grid cells with at least 15% ice concentration) enable to highlight years with
121 exceptionally low September sea-ice cover, such as 2012 and to a smaller extent
122 2007, 2016 and 2020 (Parkinson and Comiso, 2013; Petty et al., 2018; Gulev et al.,
123 2021 in IPCC, their Figure 2.20; Bushuk et al., 2024) or quantify long-term trends.
124 For instance, the September SIE exhibits a decreasing trend of -12.7 ± 2.0 % per

decade over the period 1979 to 2020 (Meier and Stroeve, 2022). However, trends of SIA or SIE only inform about changes in regime from ice to open-ocean and do not consider changes in sea-ice features.

Two main diagnostics have been proposed to document these changes. First, the age of sea-ice categorizes sea-ice into three types: open-water, first-year ice and multi-year ice (Kwok et al., 2007; Regan et al., 2022). Maslanik et al. (2011) show a strong decrease in the proportion of multiyear ice in the Arctic Ocean during the 1980-2011 period, especially in the Canadian sector. A second diagnostic deals with the duration of the ice-free period, and quantifies the timing of the transition between the freezing and melting seasons. The recent Arctic sea-ice reduction has resulted in a longer ice-free season (~ 5-10 days per decade), due to both earlier ice retreat and later ice advance (Stammerjohn et al., 2012; Stroeve et al., 2014; Lebrun et al., 2019), especially in the Chukchi, East Greenland and northeast Barents seas (Markus et al., 2009; Parkinson, 2014; Johnson & Eicken, 2016). However, these diagnostics do not consider the full seasonal cycle of sea-ice, and thus do not inform on the sea-ice dynamics including melting and growth behaviour.

These three ways of describing the variations in Arctic SIC (trend of SIE, sea-ice age, ice-free duration), without considering directly the full sea-ice seasonal cycle, have nonetheless highlighted changes in the shape of the sea-ice seasonal cycle: (i) the trend in SIE depends on the season, being maximum in late summer (Fox-Kemper et al., 2021 in IPCC, their Figure 9.13; Meier and Stroeve, 2022), (ii) Arctic sea ice has shifted to younger ice between 1979 and 2018 (IPCC, 2019) and (iii) the trend of later ice advance is expected to eventually double that of earlier retreat over this century, shifting the ice-free season into autumn (Lebrun et al., 2019). Here, in this paper, we describe the evolution of the Arctic by delimiting spatio-temporal regions having a common type of seasonal cycle.

Regionalizations of the Arctic have been proposed previously. Parkinson et al., (1978) divided the Arctic into 8 regions based on either geographical boundaries or physical criteria (e.g.; the Central Arctic encompassing the largest mass of perennial sea-ice or the Greenland Sea which allows for the only deep-water connection within the Arctic Basin). This regionalization was expanded by splitting regions into

individual seas to distinguish the behaviour of the Arctic coastal regions, resulting in considering up to 15 or 18 regions (Meier et al., 2007; Peng and Meier, 2018). Besides, five climatic regions of the Arctic have been defined using multiannual averages of a number of meteorological elements computed for the first half of the 20th century: Atlantic, Siberian, Pacific, Canadian and Baffin Bay regions (Przybylak, 2002, 2007). Other regionalizations have been used to assess the influence on lower latitude climates of Arctic sea-ice loss from specific areas (5 to 7 regions; Levine et al., 2021; Delhay et al., 2024). However, the criteria for the boundaries of these proposed regions are hard to determine and somewhat arbitrary. A statistical regionalization method based on observed SIC has been proposed for Antarctica. Raphael and Hobbs, (2014) isolates regions around Antarctica by using sea ice extent decorrelation length scale and variance. The resulting five sectors exhibit distinct times of sea-ice advance and retreat. Their methodology does not account for the temporal evolution of the sectors. The originality of our analysis resides in the fact that we regionalize the Arctic based on physical criteria of the dynamics of the sea-ice seasonal cycle, therefore without imposing pre-defined regions and allowing the regions to evolve in time. To do so, we set up a clustering method (unsupervised machine learning).

Regionalizations determined from clustering methods applied to ocean temperature profiles have been shown to be an efficient tool, to capture coherent physical changes of e.g. the water column during an El Niño event (Houghton and Wilson, 2020) or heat distribution in the North Atlantic (Maze et al., 2017). The same conceptual methodology has also been applied to the polar regions. In the Antarctic, Wachter et al. (2021) described the spatio-temporal sea-ice variability and documented significant spatial shifts during 1979-1998 and 1999-2018 by means of 10 clusters based on the seasonal cycle of sea-ice. In the Arctic, Valko (2014) proposed a regionalization based on geographic and geopolitical indicators, ending up with respectively two and three clusters, and Johannessen et al. (2016) identified 6 major regions by clustering annual average of surface air temperature. The boundaries of the defined clusters coincide with the outlines of the continents and the averaged position of the sea-ice edge. Besides, clustering methods for other purposes than regionalization have been used in the Arctic. Gregory et al., 2022 using

188 a clustering analysis together with complex networks, show that climate models
189 underestimate the importance of some regions (Beaufort, East Siberian, and Laptev
190 seas) in explaining the pan-Arctic summer SIA variability. Using an ocean-sea ice
191 general circulation model, Fuckar et al. (2016) performed a k-means cluster analysis
192 on pan-Arctic detrended sea-ice thickness and found that the associated binary time
193 series of cluster occurrences exhibit predominant interannual persistence with a
194 mean timescale of about 2 years. However, no spatio-temporal regionalization based
195 on the clustering of the Arctic seasonal cycle of sea-ice has been proposed so far.

196 In this paper, we determine Arctic regions based on statistically different
197 sea-ice concentration seasonal cycles, and describe Arctic changes through the time
198 evolving borders. We identify for the first time spatio-temporal regions of the Arctic
199 based on the variability of the seasonal cycle of Arctic sea-ice concentration. We
200 apply a k-means clustering method to determine regions based on their time-evolving
201 belonging to a given type of seasonal cycle. In section 2, the dataset, domain of
202 interest and clustering method are detailed. In section 3, we first analyze the
203 clustering outputs of the Arctic sea-ice seasonal cycle (3.1), then examine the
204 probability to belong to each cluster (3.2), and finally investigate the regime stability
205 and transition (3.3). Conclusions and discussion follow in section 4.

206

207 2. Data and Clustering Method

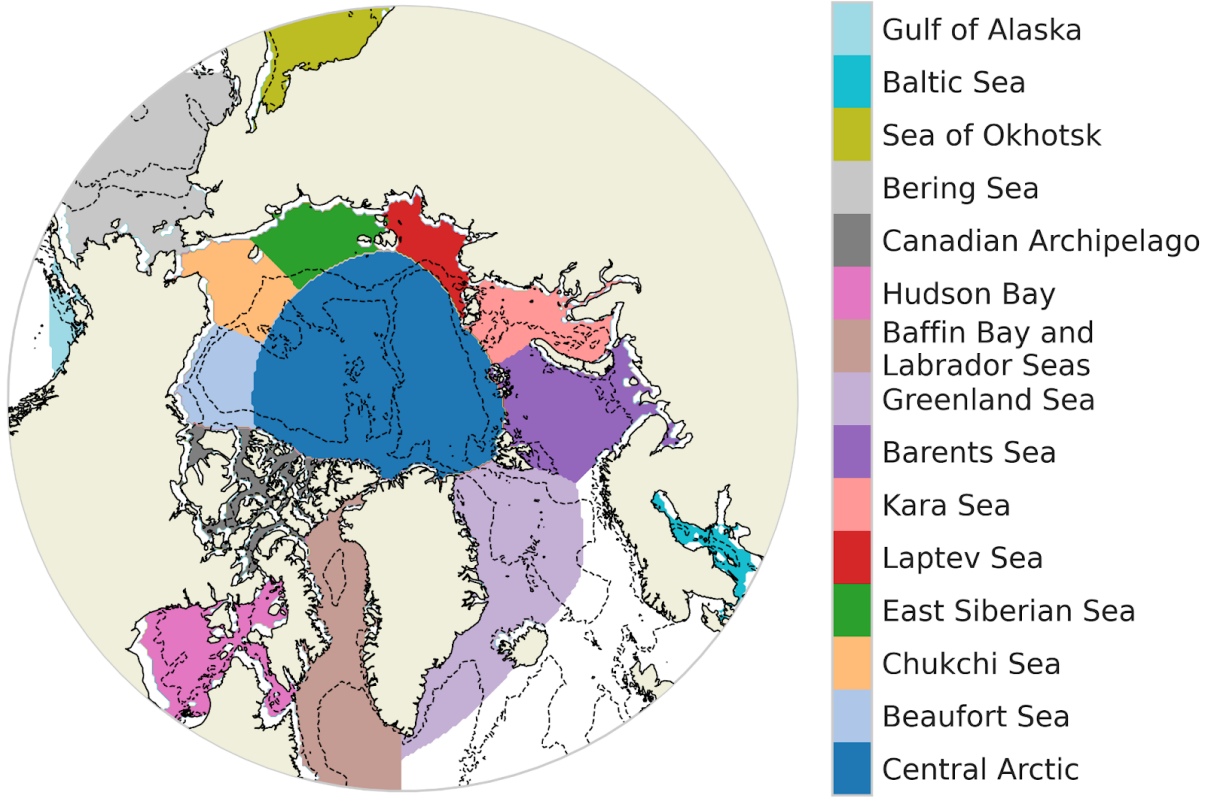
208 2.1 Sea-ice concentration (SIC)

209 The National Snow and Ice Data Center (NSIDC) provides gridded SIC fields on
210 a 25 km polar stereographic projection obtained from passive microwave satellite
211 measurements on daily temporal resolutions. We use the climate data record (CDR)
212 product (Meier et al., 2021), which is based on the most recent approach combining
213 the NASA team (NT; Cavalieri et al., 1984) and the bootstrap (BT; Comiso et al., 1986)
214 algorithms. Because of the tendency of passive microwave measurements to
215 underestimate concentration, the CDR chooses the higher concentration between
216 the NT and BT algorithms and assigns it to each grid cell. The pole hole - the region
217 around the North Pole where satellite measurements are unavailable - is filled from

the average concentration of the circle of surrounding adjacent grid cells. The size of the pole hole has diminished over time due to advancements in satellite technology. Measurement uncertainties are highest at low SIC, where satellite signals are often influenced more by atmospheric and surface conditions—such as clouds, water vapor, melt on the ice surface, and changes in the character of the snow and ice surface—than by the actual presence of ice. We utilize daily data from January 1979 to December 2023, using linear interpolation for the few missing data and compute mean values every 5 days. The 29 February of every bissextile year is removed before computing the 5-day mean. We choose this 5-day temporal resolution as similar results are found for a daily temporal resolution whereas a monthly temporal resolution shows small differences in the spatial distribution of clusters (Figure S1). Throughout the manuscript, sea-ice will always relate to concentration.

2.2 Studied domain

The study considers the ocean above 55°N. The description of the domain is based on the delimitation provided by NSIDC (Meier et al., 2023) and encompasses 15 classically predefined regions (Figure 1). The bathymetric data is derived from the GEBCO 2024 Grid (GEBCO Compilation Group, 2024).



237

238 Figure 1: Geographical decomposition of the Arctic Ocean (defined as ocean above
 239 55°N) into 15 regions following Meier et al. (2023). Bathymetry contours -100 m and
 240 -2000 m are drawn with a dotted line.

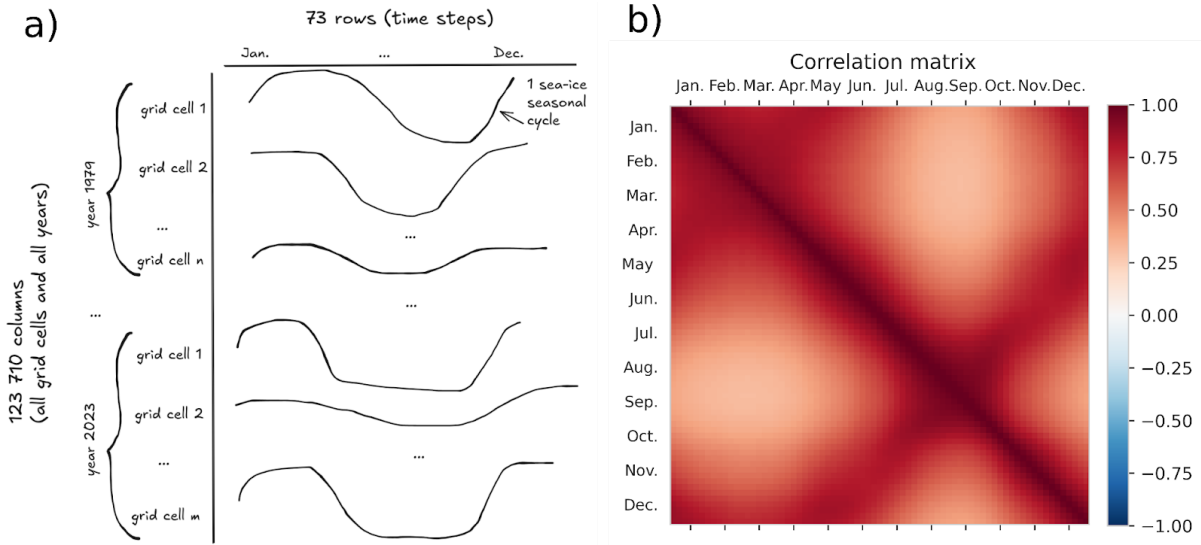
241

242 2.3 Clustering set up

243 We consider all oceanic grid cells above 55°N having a non-zero sea-ice
 244 seasonal cycle (having at least a non-zero value for SIC throughout the year). Hence,
 245 the number of considered grid cells depends on the year. Grid cells with a zero
 246 sea-ice seasonal cycle are reintroduced after the clustering in order to define an
 247 open-ocean cluster. This favours a separation between regimes with and without
 248 sea-ice. The input data of our clustering are all the seasonal cycles including every
 249 considered grid cell and every year. In practice, we are thus working with a matrix
 250 with rows containing every considered grid cell of the period 1979-2023, here called
 251 points (1123710 elements) and columns containing every time step for one year, here

252 5-day mean (73 elements). A schematic of this matrix input data for the clustering is
253 presented Figure 2a.

254 We implement a k-means clustering algorithm, which is an unsupervised
255 machine learning method that groups data into subsamples sharing common features
256 (Jain et al., 2010). It has the advantage of being non-parametric as our data
257 distribution is strongly non-Gaussian. Indeed, SIC is bounded between 0 and 1 with
258 high occurrences of values close to 0 and 1. It is an iterative method that minimizes a
259 cost function being the sum of the squared distance (distance in a sense that would
260 be defined later) between each seasonal cycle and its nearest cluster center (also
261 called centroid). At each iteration, the coordinates of the centroids are updated. The
262 initialization of centroids coordinates using k-means++ concept (the first centroid is
263 chosen randomly, the second is the farthest-away, the third the farthest-away of the
264 first and second, and so on) has been tested and is partly impacting our results.
265 Therefore, we choose a different initialization strategy. We initialize the centroids
266 coordinates based on seasonal cycles that separate the data into equal quantiles. For
267 a clustering involving two clusters, the initializations are the two seasonal cycles of
268 0.33 and 0.66 quantiles of all seasonal cycles; for a clustering involving three clusters,
269 the initializations are the three seasonal cycles of 0.25, 0.5, and 0.75 quantiles, and so
270 on (Figure 3b). The quantiles are calculated over all the seasonal cycles considered in
271 this study. This favours initial centroids far from each other to avoid iterating over a
272 local minimum and the clustering is thus deterministic (i.e., it does not present any
273 random aspect). The strategy of initialization based on quantiles has been
274 investigated for synthetic and real dataset and has shown a faster convergence
275 compared to random and Kmeans++ initialization techniques (Jambudi and Gandhi,
276 2022).



277

278 Figure 2: Schematic of the matrix input data for the k-means clustering (panel a) and
 279 correlation matrix of the 5-day mean SIC for all non-zero sea-ice seasonal cycle above
 280 55°N (panel b)

281

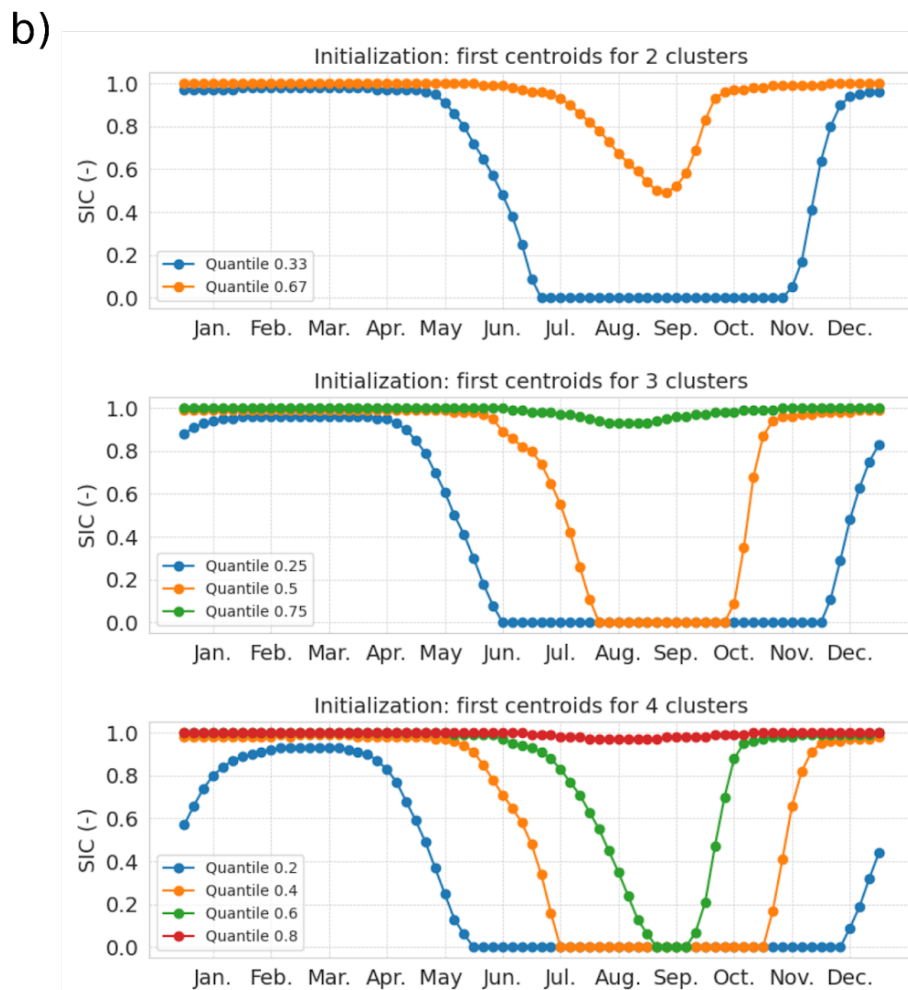
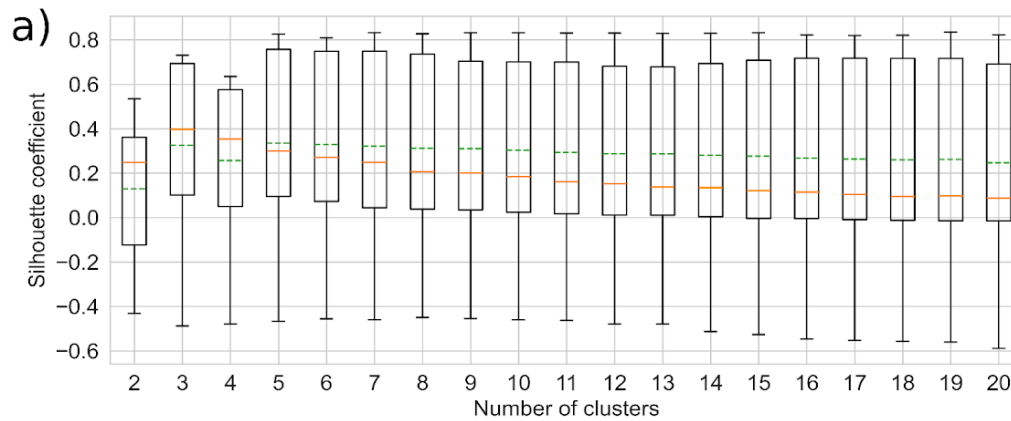
282 The clustering algorithm is based on the calculation of distances. The
 283 Euclidean distance is often used in similar methods, yet, here, we choose to use the
 284 Mahalanobis distance (using the correlation matrix) to constrain the clustering with
 285 physical information. All the combinations of 5-day mean SIC have a positive
 286 correlation, as shown in Figure 2 by the correlation matrix. The correlation matrix is
 287 computed for all nonzero seasonal cycles for the period 1979-2023 above 55 °N. It is
 288 calculated from the matrix of shape (73, 1123710), having 1123710 value of SIC for
 289 73 dates. Notably, a strong correlation exists between spring and autumn (June and
 290 November), while the weakest correlations are between summer and winter (March
 291 and September, minimum correlation is 0.31). As data are correlated, a privileged
 292 direction exists when plotting the SIC for all grid cells and all years of a given date
 293 (5-day mean) against another date. We consider this physical relation of temporal
 294 dependency by using the Mahalanobis distance (which we defined as an Euclidean
 295 scalar product normalized by the inverse of the correlation matrix) in the clustering
 296 algorithm. A 5-day mean SIC strongly correlated with another (such as spring and
 297 autumn) has a reduced distance compared with Euclidean distance. We note that, as
 298 we want to conserve the physical information of the variability intensity for each
 299 5-day mean SIC, we do not normalize the distance by the covariance matrix (as
 300 usually done for the Mahalanobis distance) but by the correlation matrix that only

301 takes into account relation between different 5-day mean SIC. As a result, a 5-day
302 mean SIC with weak variability (as in winter) will have a smaller impact on the total
303 seasonal cycle than a 5-day with larger variability (as in summer). Therefore, we do
304 not modify the relative weight (based on the variability) of each 5-day mean SIC.

305 The Mahalanobis norm, deriving from a symmetric operator, effectively rotates
306 the original physical phase space (here, date of the annual cycle) to align with the
307 data's natural directions—linear combinations of the physical time axis. This
308 transformation allows centroid detection in a space that reflects the intrinsic
309 structure of the data. Therefore, using the Mahalanobis distance helps the clustering
310 algorithm to follow the direction of the correlation and capture the elongated shapes
311 of clusters. When calculating the probability to belong to one cluster, we do not need
312 to work with the data's natural directions, but rather work in the original physical
313 time space. Therefore we use Euclidean distance for the calculation of probability and
314 the Mahalanobis for the clustering.

315 The number of clusters needs to be specified for the k-means clustering. We
316 define the optimal number of clusters based on the Silhouette coefficient
317 (Rousseeuw, 1987; Houghton and Wilson, 2020) that measures the quality of the
318 clustering when seeking for compact and well-separated clusters. We rely on the
319 `Silhouette_sample` function from the python package `sklearn.metrics` (Pedregosa et
320 al., 2011), which calculates the Silhouette coefficient for every point as $(b - a) / \max(a, b)$
321 where a is the mean intra-cluster distance and b is the mean nearest-cluster
322 distance for each point. Each point is labelled as being in a cluster using the k-means
323 clustering (with correlation-based Mahalanobis distance), while the distance used in
324 the calculation of a and b is the Euclidean distance. The larger the Silhouette
325 coefficient is (bounded between -1 to 1), the farthest the centroids are from each
326 other and the more grouped are the points of the same cluster. We have computed
327 the Silhouette coefficient for 18 clustering (number of clusters ranging from 2 to 20;
328 Figure 3). As the distribution of the Silhouette coefficient is asymmetric, we sort this
329 sensitivity test using the median. The maximum median Silhouette coefficient gives
330 an optimal number of clusters, which is three in our case (Figure 3a). Therefore, after
331 reintroducing the open-ocean grid cell for each year, we end up with four clusters

332 (three optimal clusters obtained using the Silhouette coefficient for non-zero seasonal
 333 cycle of sea ice and the open-ocean cluster reintroduced manually).



334

335 Figure 3: Boxplot of the Silhouette coefficient for a number of clusters from 2 to 20.
 336 The box extends from the first quartile (0.25) to the third quartile (0.75) of the
 337 Silhouette coefficient. The whiskers indicate the 1st and 99th percentiles. The

green-dashed and orange-solid lines indicate the mean and median values, respectively (panel a). Equal quantile separation initialization: centroids of the first iteration of the clustering for a number of cluster of 2, 3 and 4 (panel b)

3. Results

3.1 Clustering outputs

The clustering method connects each seasonal cycle to a given cluster (Figure 4a) and provides the centroids of each cluster (Figure 4b). As shown in Figure 4a for year 1979 and 2023, the clustering method associates the sea-ice seasonal cycle of each year and each grid cell to the nearest seasonal cycle type (based on the smallest Mahalanobis distance between the seasonal cycle of the point and the seasonal cycle of the centroids). Without giving any information to the clustering algorithm on the spatial and temporal dependency between the seasonal cycles, we retrieve spatially continuous patterns. The clusters are sorted going toward the pole as follows: the open-ocean cluster, the partial winter-freezing cluster, the full winter-freezing cluster and the permanent sea-ice cluster. The first three clusters exhibit wavy bands surrounding the pole, and the permanent sea-ice cluster sits over the pole. More details on the description of the regions will follow based on our probabilistic framework (section 3.2).

The centroids (Figure 4b) of a cluster correspond to the average of all seasonal cycles belonging to the cluster. It is referred to as the type of seasonal cycle. They exhibit the expected physical behavior that, due to the thermal inertia of the ice and indirect processes involving the ocean and atmosphere, the maximum sea-ice coverage (in March) follows the minimum solar insolation by a lag of around 3 months, and the minimum sea-ice coverage (in September) occurs around 3 months after the maximum solar insolation (Parkinson et al. 1987).

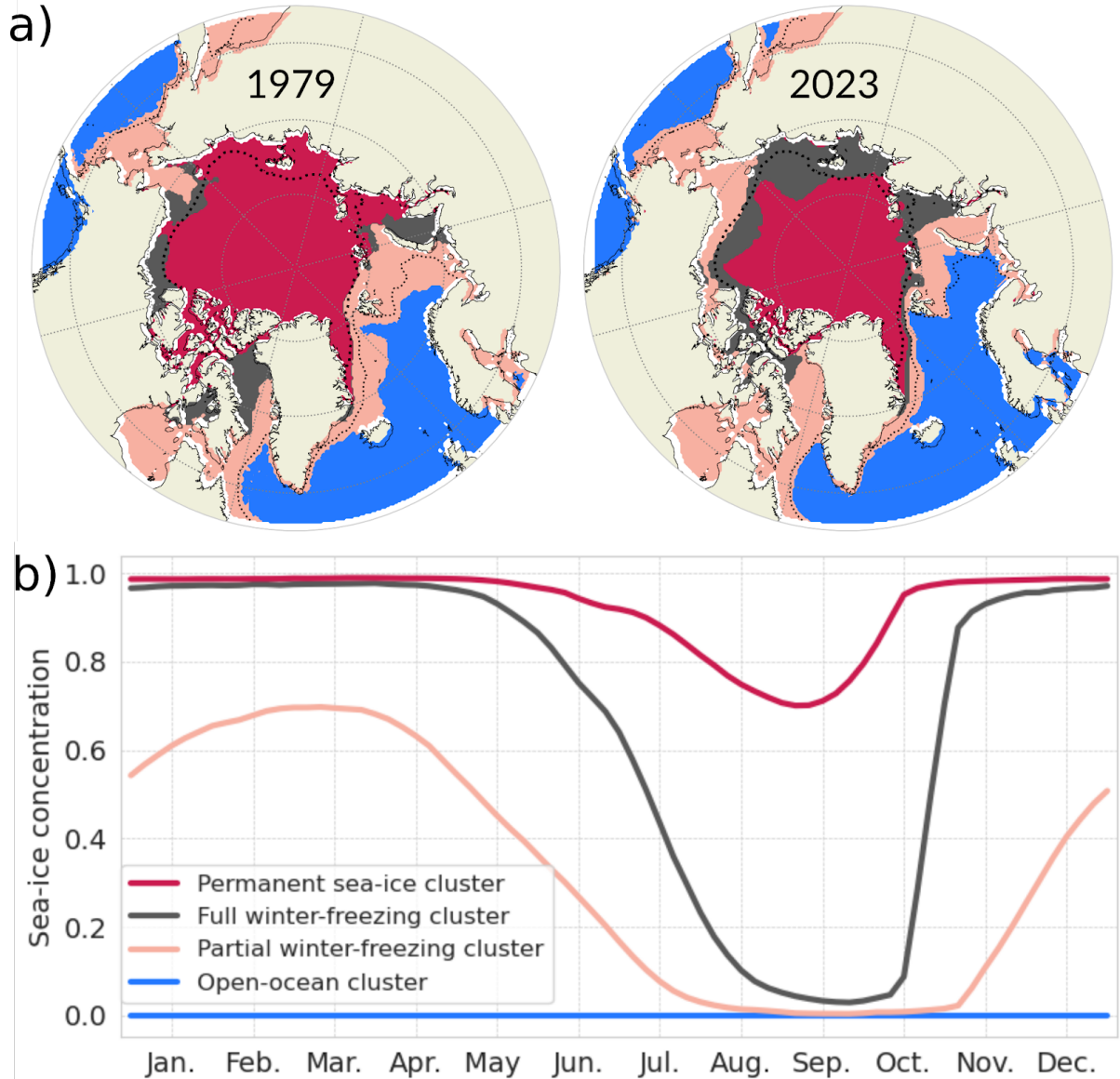
The four types of seasonal cycles present different features. The open-ocean cluster has a SIC equal to zero all year round, which was sought for our analysis and

367 represents year-long ice-free conditions. We refer to ice-free conditions when SIC is
368 below 0.15. The second cluster, referred to as partial winter-freezing, has a
369 quasi-sinusoidal shape with a mean SIC ranging from ~70% in March to no-ice in
370 summer (early August to mid-October). The full winter-freezing cluster is bound to a
371 SIC of 100% from mid-November to April and to almost no-ice by mid-September.
372 For this cluster, the sea ice completely melts in 5 months (from April to September)
373 and totally freezes up in 2 months (from mid-September to mid-November). The full
374 winter-freezing cluster has more abrupt seasonal changes compared to the partial
375 winter-freezing cluster. The permanent sea-ice cluster has sea ice covered all year
376 round, with only a partial melting between May and October, peaking at its minimum
377 in late August (mean SIC around 70%).

378

379

380



381

382 Figure 4: (a) Four types of seasonal cycles (output of the clustering method, called
 383 centroids) (b) their corresponding regions for the years 1979 (left) and 2023 (right).
 384 The dotted thin and thick lines are the mean SIC of 0.15 and 0.8 for the period
 385 1979-2023, respectively.

386 This clustering analysis shed light on sea ice precursors for fully covered ice
 387 conditions and ice-free conditions, as the three clusters with sea ice have different
 388 first dates of retreat and first dates of advance. In our optimal data separation
 389 analysis, it appears that when considering areas totally covered by ice in winter
 390 (permanent and full winter freezing clusters), the first date of retreat is a good
 391 indicator for ice-free conditions in summer. Considering a given location fully

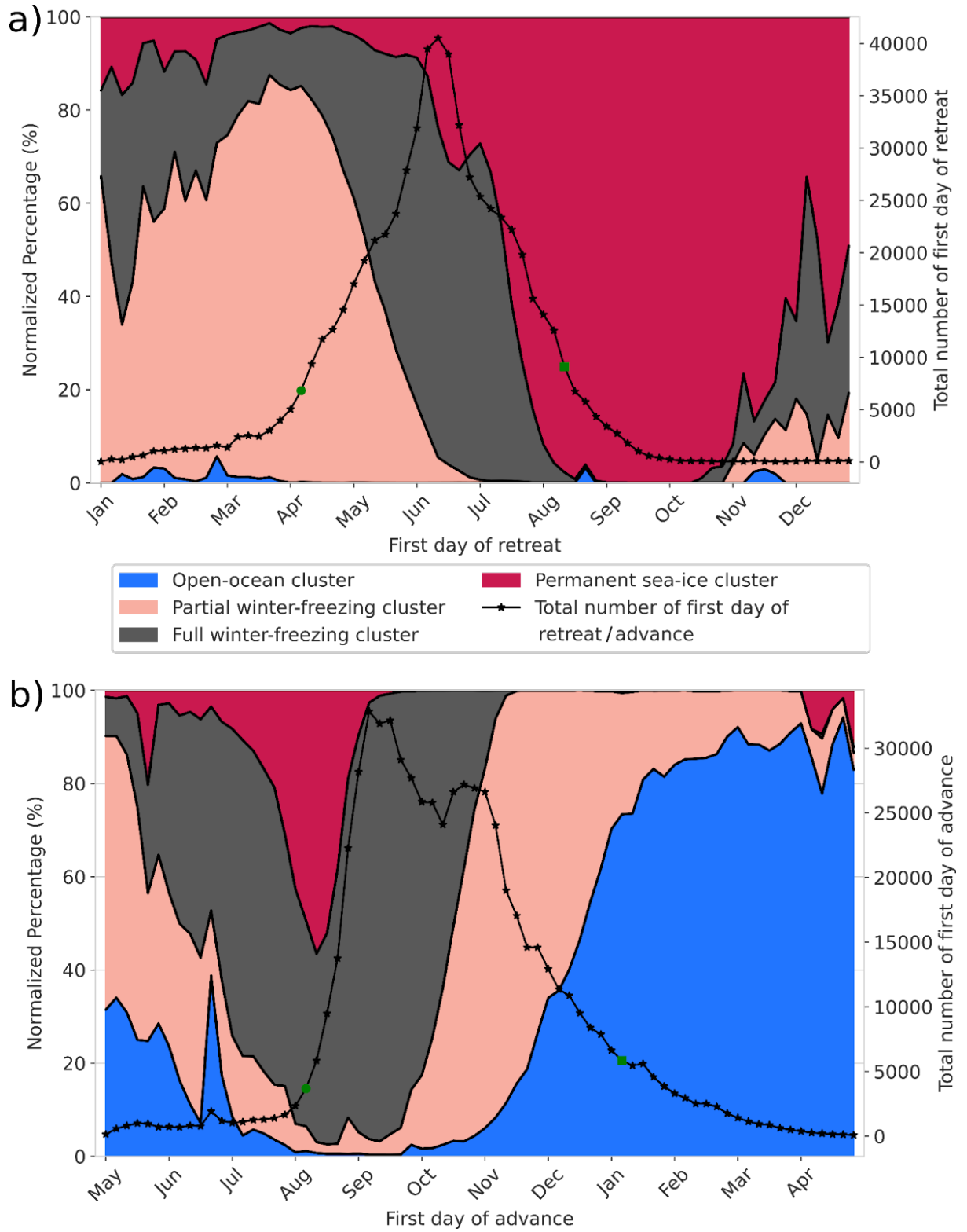
ice-covered in a given winter, our clustering results suggest that when the sea ice starts to melt in April, the seasonal cycle belongs to the full winter-freezing cluster and be ice-free the next summer. In contrast, when the melting starts one month later (in May) the seasonal cycle belongs to the permanent sea-ice cluster and the considered location will not be ice-free in summer. Besides, the freezing date for areas free of ice could differentiate between the partial winter-freezing and full winter freezing clusters and subsequently predict full ice conditions in the following winter. In our clustering, a freezing starting in October totally freezes in winter which is not the case if the freezing starts in November, having a maximum of about 70% SIC in March. Therefore, it seems that, for ice-free conditions in summer, the first date of advance is a good indicator for full ice conditions in the next winter.

However, this suggestion relies solely on the shape of the four types of seasonal cycles but to properly quantify this, the spread must be taken into account. Figure S2 displays the spread of the seasonal cycle by plotting the quantiles 0.1, 0.5 and 0.9 of each cluster. To verify our hypothesis on sea-ice indicators, we account for the spread of the date of retreat and date of advance for each cluster. To do so, we calculate the first date of retreat (the first date after the maximum SIC that is below 0.9) for each seasonal cycle experiencing fully ice covered conditions (having at least one value above 0.99 during the year). We also calculate the first date of advance (the first date after the minimum SIC that is above 0.1) for each seasonal cycle experiencing ice-free conditions (having at least one value below 0.01 during the year). For these calculations, seasonal cycles have been temporally filtered using a 15 days sliding window in order to get rid of short-term dynamical ice events, as done in Lebrun et al., (2019). To circumvent the effect of the discontinuity between 31 December and 1 January, we define the origin of time in May for the calculation of the date of advance. We then label each first date of retreat and first date of advance for each seasonal cycle with its corresponding cluster according to our clustering analysis (Figure 4a).

The normalized probability over each cluster of the first date of retreat and first date of advance at each date is shown Figure 5. This figure also displays the total number of the first date of retreat and the first date of advance of all clusters for each

423 date. If the first date of retreat occurs between January and April, there is around
424 95% of chance to belong to either the open-ocean cluster, the partial winter-freezing
425 cluster or full winter freezing cluster, which all present ice-free duration in the
426 following summer. However, this situation did not often occur, as the total first date
427 of retreat happening in this period is unlikely (solely around 5% of first date of retreat
428 for all clusters). The first date of retreat is more likely to occur between the beginning
429 of April and August, as within this period around 90% of the total date of retreat for
430 all clusters exist. A first date of retreat in early July has around 70% of chance to
431 belong to the full winter-freezing cluster which present ice-free conditions in summer
432 while a first date of retreat in early August has around 90% of chance to belong to
433 the permanent sea-ice cluster which doesn't show ice-free conditions in summer.

434 The first date of advance is more likely to occur between the beginning of
435 August until the beginning of January, as within this period around 90% of the total
436 date of advance for all clusters exist. A first date of advance in early September has
437 around 95% of chance to belong to the full winter freezing cluster which present fully
438 ice covered condition in the following winter, while a first date of advance in early
439 November has around 80% of chance to belong to the partial winter-freezing or open
440 ocean clusters which do not show fully ice covered conditions in the following winter.
441 Therefore, this simple model suggests that the first date of retreat could be a good
442 indicator for ice-free conditions the following summer and the first date of advance a
443 good indicator for fully ice cover conditions the following winter.

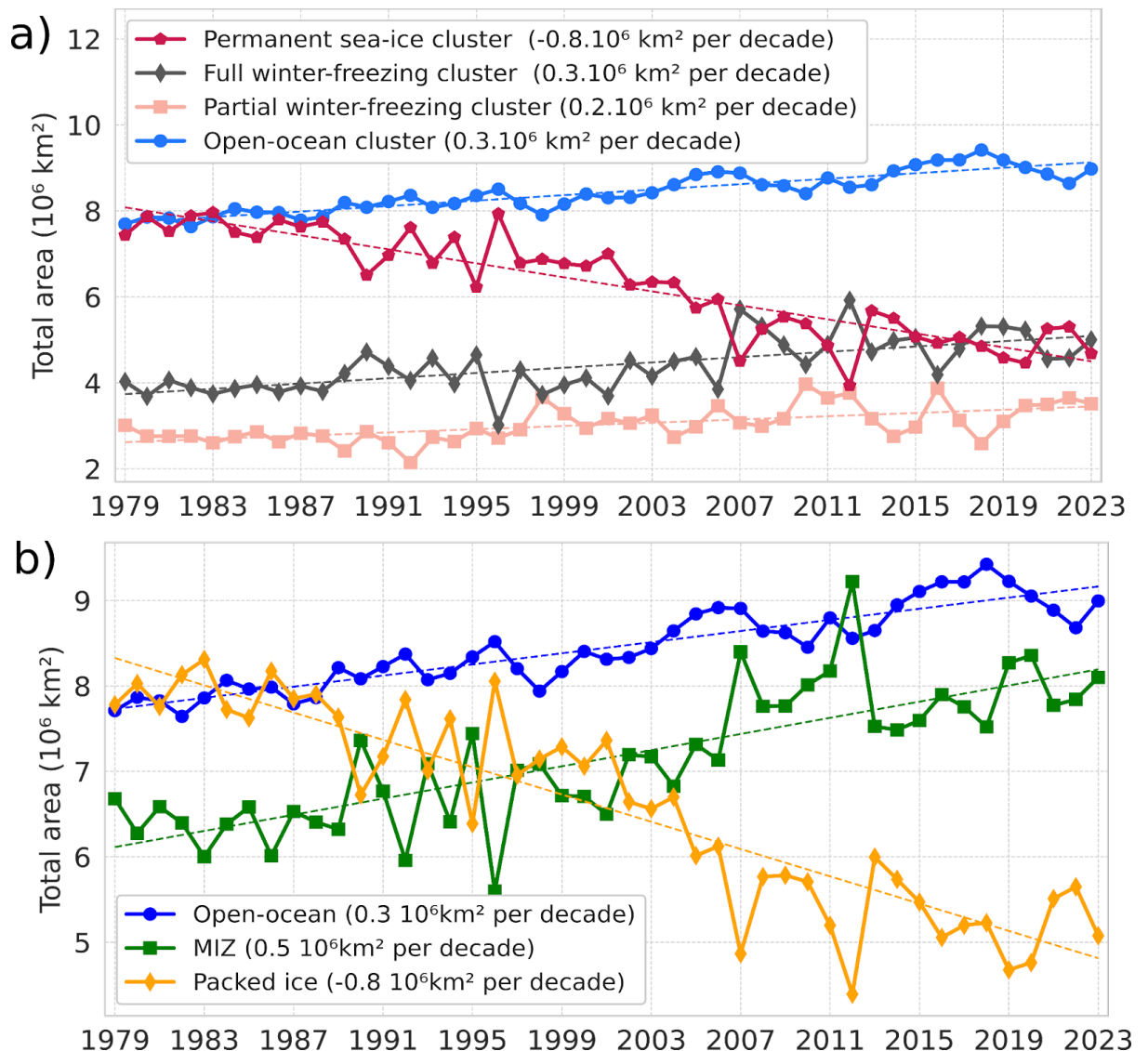


444

445 Figure 5: Normalized probability of the first date of retreat (panel a) and first
 446 date of advance (panel b) for each cluster. The solid lines with star markers are the
 447 total number of first dates of retreat and first dates of advance for all clusters. The
 448 green circle markers (start date) and green square markers (end date) cover the

449 shortest period where around 90% of the first date of retreat, respectively the first
 450 date of advance, for all clusters occurs.

451 To emphasize the added value of our clustering, we compare it to a more
 452 classical classification (Figure 6b) in which the sea ice cover is separated into the
 453 packed ice category ($0.8 < \text{SIC} < 1$), the Marginal Ice Zone (MIZ; $0.15 < \text{SIC} < 0.8$) and
 454 the remaining, open-ocean category ($\text{SIC} < 0.15$; Aksenov et al. 2017). The thresholds
 455 of 0.15 and 0.8 to define the MIZ are convenient to represent a category with loose
 456 and packed ice but somehow arbitrary and other definitions of the MIZ have been
 457 proposed in the literature based on dynamical considerations (e.g. Sutherland and
 458 Dumont 2018). Using the cluster vision, we compute the evolution of the total area
 459 corresponding to each of our four clusters (Figure 6a).



460

Figure 6: (a) Time series of the total area covered by each of the four clusters. (b) Times series of the area covered by three categories: packed ice ($0.8 < SIC < 1$), the Marginal Ice Zone (MIZ; $0.15 < SIC < 0.8$) and the open-ocean ($SIC < 0.15$). All curves show a significant linear trend with a p-value less than 0.05 using a Wald Test with a t-distribution.

These two methods (Figure 6a and Figure 6b) both indicate a shift toward more seasonal and ice-free conditions. Indeed, in the clustering method the permanent sea-ice cluster has notably decreased of the same amount than the packed ice in the classical categorization ($-0.8 \cdot 10^6 \text{ km}^2$ per decade). Also, the open-ocean cluster follows the same trend of the open-ocean category ($0.3 \cdot 10^6 \text{ km}^2$ per decade). The increase in the area of MIZ category is around $0.5 \cdot 10^6 \text{ km}^2$ per decade and has been demonstrated previously (Cocetta et al., 2024; Song et al., 2025). Therefore, it appears with our clustering that the MIZ is refined into two clusters : the full winter-freezing ($0.3 \cdot 10^6 \text{ km}^2$ per decade) and the partial winter-freezing cluster ($0.2 \cdot 10^6 \text{ km}^2$ per decade). This suggests that the tendency is more likely to shift to a more abrupt melting and growth seasonal cycle (full winter-freezing cluster) compared to a quasi-sinusoidal sea-ice seasonal cycle (partial winter-freezing cluster) or, in other words, that the tendency is more likely to a total ice cover in winter with a short ice-free season (2 months, full winter-freezing cluster) than a partial ice cover in winter with a long ice-free season (4 months, partial winter freezing cluster).

Also, looking at the years with marked extremes in September sea ice extent, (2007, 2012, 2016 and 2020; see introduction), the MIZ categorization shows a transfer of area between the packed ice and the MIZ. In our clustering vision, 2007, 2012 and 2020 show a transfer of area between the permanent sea-ice cluster and full winter-freezing cluster while 2016 show a transfer of area between the full winter-freezing and the partial winter freezing, reflecting different dynamical changes in the sea-ice seasonal cycles. Therefore, our clustering analysis presents a more detailed description of the MIZ category.

As a given seasonal cycle can be in between two or more seasonal cycle centroids, we introduce the probability to belong to one cluster in the next section.

3.2 Probability to belong to a cluster

3.2.1 Calculation

To calculate the probability P of a grid point to belong to each cluster. We define the vectors \mathbf{x} and $\mathbf{c}(\mathbf{k})$, corresponding respectively to the SIC observed at a grid cell over a year (i.e., 73 intervals of 5 days) and the cluster centroid k . These are of dimension (73x1) and are written as:

$$\begin{aligned} \mathbf{x} &= [x_1, \dots, x_{73}]^T; \\ \mathbf{c}(\mathbf{k}) &= [c_1(k), \dots, c_{73}(k)]^T \end{aligned} \quad (1)$$

The Euclidean distance scalar between the point \mathbf{x} and the centroid k is defined as follows:

$$d_{x,c(k)} = \sqrt{(\mathbf{x} - \mathbf{c}(\mathbf{k}))^T (\mathbf{x} - \mathbf{c}(\mathbf{k}))} \quad (2)$$

The probability P reads:

$$P(x, k) = \left[\sum_{l=1}^{n_c} \left(\frac{d_{x,c(k)}}{d_{x,c(l)}} \right)^2 \right]^{-1} \quad (3)$$

with n_c the total number of clusters (four in our case). P ranges from 0 to 1 and the sum over the four clusters of P equals 1. In other words, the probability of being in a cluster is set by the distance of one seasonal cycle to a seasonal cycle centroid, normalized by the sum of the Euclidean distance to all clusters. This means that we use a “fuzzy” k-means clustering where the assignment is soft (each data point can be a member of multiple clusters) in contrast to a hard or crisp assignment (each data point is assigned to a single cluster; Jain et al., 2010).

We call the total probability, P_t , the normalized area weighted probability over all grid cells. We sum, for each year, the probability weighted by the area of each grid

cell over all grid cells divided by the sum of the probability weighted by the area of each grid cell over all clusters and all grid cells. P_t can be written as:

$$P_t(k) = \frac{\sum_x P(x,k) \cdot \text{area}(x)}{\sum_k \sum_x P(x,k) \cdot \text{area}(x)} \quad (4)$$

3.2.2 Trend of the pan-Arctic probability to belong to a cluster

After attributing each point to a probability of belonging to each cluster per year (using equation (4)), we analyze in a spatially integrated way the pan-Arctic evolution of the total probability to belong to a cluster (normalized area-weighted probability). The probability of belonging to the open-ocean cluster is around 40%, to the permanent sea-ice cluster is around 29% and to the full winter-freezing cluster is around 18 % and to the partial winter-freezing cluster is around 13% (Figure 7). Note that the absolute value reflects our choice of domain, here above 55 °N.

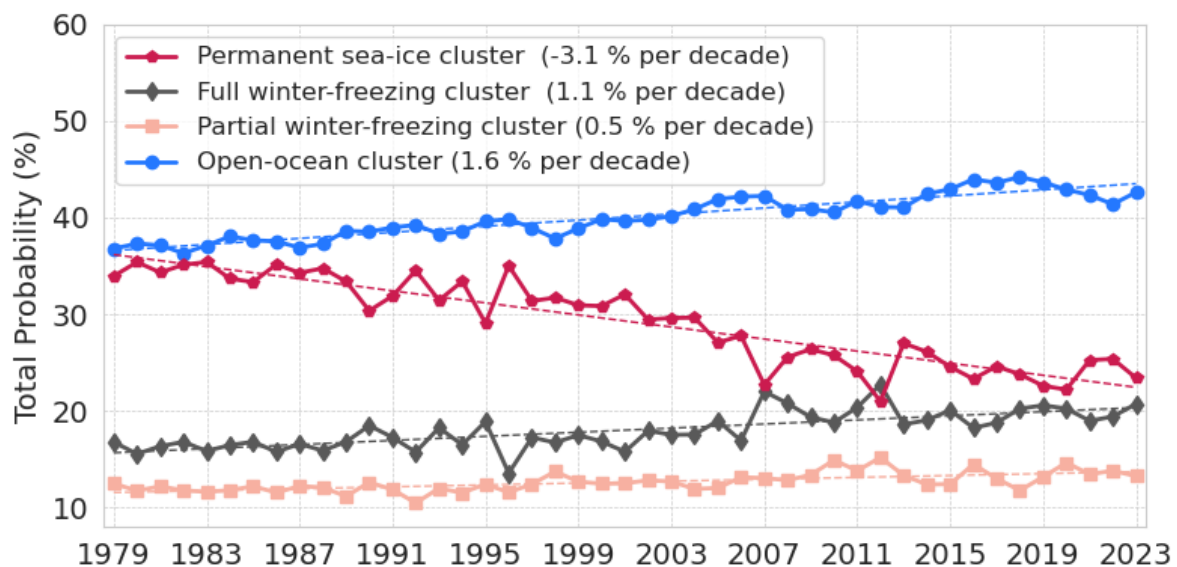


Figure 7: Evolution of the total probability (see Equation (4)) to belong to each cluster. All clusters show a significant linear trend with a p-value less than 0.05 using a Wald Test with a t-distribution

However, the time evolution of these clusters is in direct relation to the dynamics of the Arctic sea ice. A linear regression analysis indicates that the trends

for all clusters are statistically significant, with a p-value less than 0.05 using a Wald Test with a t-distribution. The total probability of belonging to the permanent sea-ice cluster overall declines by around 3.1% per decade with an acceleration around the 1997-2012 period. The total probability of the three other clusters shows a decline, firstly for the open-ocean cluster (1.6% per decade) and to a smaller extent full winter-freezing (1.1%) and the partial winter-freezing (0.5% per decade). Therefore, most of the pan-Arctic probability loss over the last 45 years from the permanent sea-ice cluster is compensated by a gain of the open-ocean cluster and to a smaller extent to the full and partial winter-freezing clusters.

3.2.3 Regional probability to belong to a cluster

To analyze spatial redistributions of clusters over time, we average the probability (calculated equation (3)) over three periods of 15 years (Figure 8). During the first period (1979-1993), the Nordic Seas, the Bering Sea and the Gulf of Alaska belonged solely to the open-ocean cluster (free of ice). Going northward, an outer belt shape connecting the southern Barents Sea, the northern and east Greenland Sea and the southern and east Labrador Sea in the Atlantic side and the northern Bering Sea and Sea of Okhotsk mainly belongs to the partial winter-freezing cluster. Further north, an inner belt shape tight to the Arctic coast (Beaufort Sea, Chukchi Sea, East Siberian Sea, Laptev Sea, southern Kara Sea) and to the northern Barents Sea, and Baffin Bay mainly belong to the fully winter-freezing cluster. The central Arctic predominantly belongs to the permanent sea-ice cluster. The edge of the 0.3 probability of belonging to the permanent sea-ice clusters of the period 1979-1993 follows the border of the Marginal Ice Zone (0.8 SIC) located in the Central Arctic. Some regions do not have a dominant cluster but instead have a strong probability of belonging to more than one cluster, such as the northern Kara Sea, the northern Greenland Sea and the Hudson Bay.

In the subsequent periods (1994-2008 and 2009-2023), the open-ocean cluster continuously expanded in the Barents Sea, East Greenland Sea and Labrador Sea. In these same regions, the other three clusters (partial winter-freezing, full winter-freezing and permanent sea ice clusters) retract. The permanent sea-ice

cluster exhibits substantial change, with intense shrinking from the Pacific side of the central Arctic, losing areas in a belt shape from the Beaufort Sea to the Laptev Sea which is mainly gained by the full winter-freezing sea-ice cluster. This indicates increasingly frequent summer ice-free conditions during the 1979-2023 period.

Therefore, spatial redistributions in the clusters occur over time. The permanent sea-ice retraction from the Pacific side is compensated by the full winter-freezing cluster and the open-ocean cluster expansion in the Atlantic side is compensated by loss of the partial winter-freezing cluster.

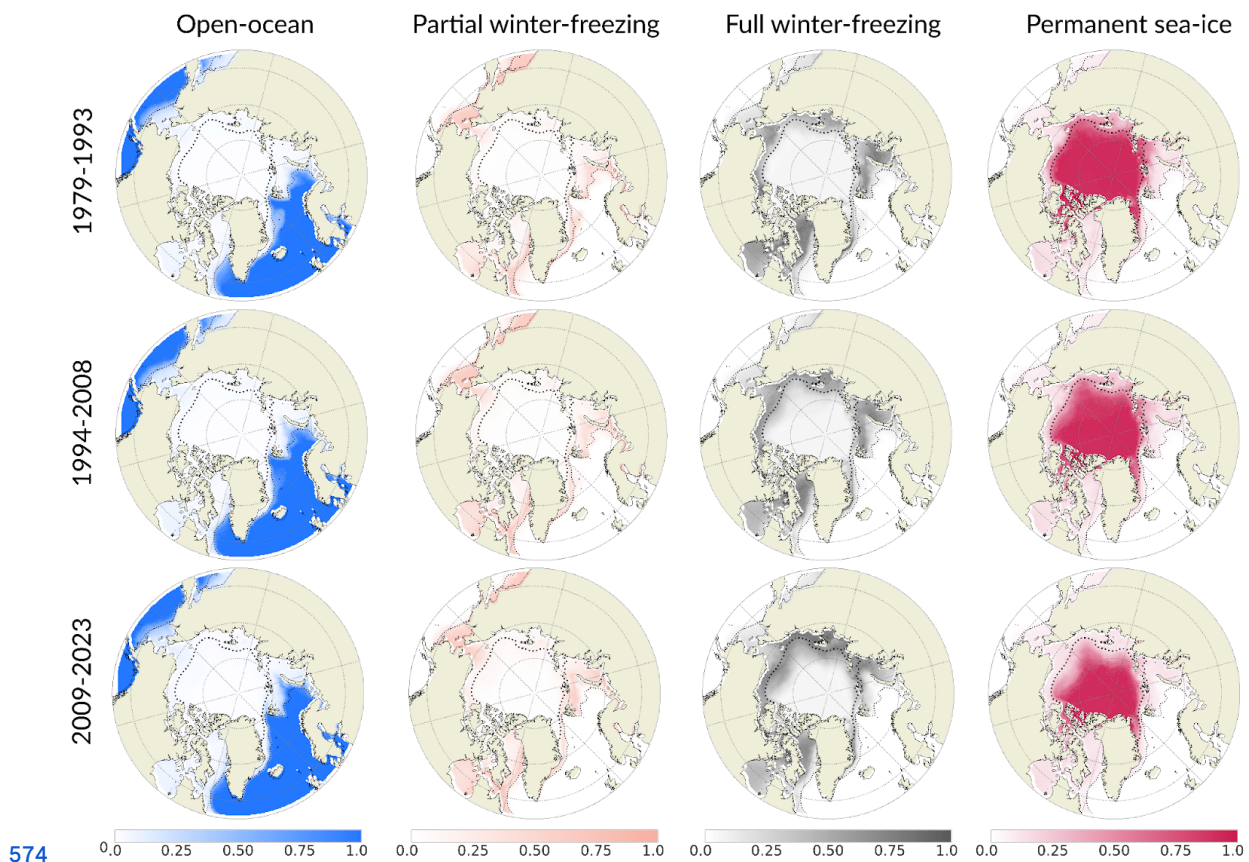


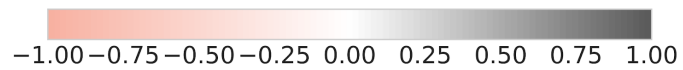
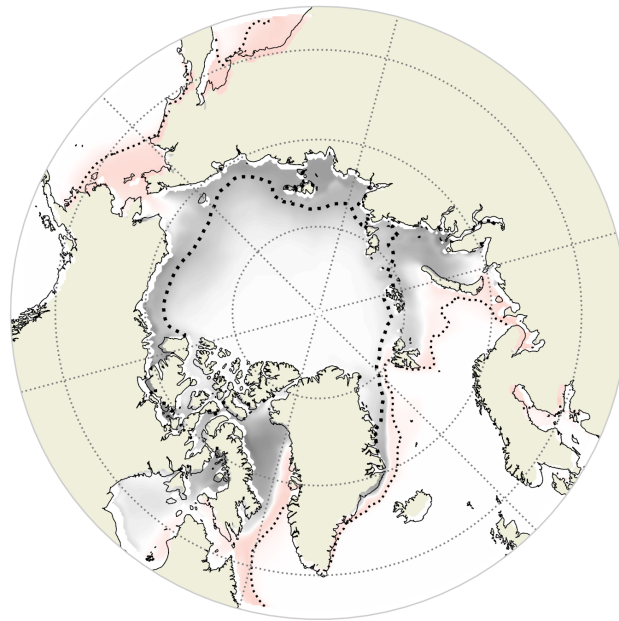
Figure 8: Map of the probability of each cluster: open-ocean (first column), partial winter-freezing (second column), full winter-freezing (third column) and permanent sea-ice (fourth column). Rows correspond to three periods of 15 years: 1979-1993 (top row), 1994-2008 (middle row) and 2009-2023 (bottom row). The dotted thin and thick lines are the mean SIC of 0.15 and 0.8 for the period 1979-2023, respectively. The circle sitting over the north pole is the pole hole (see section 2.1).

582 Therefore, over the whole period (1979-2023) the open-ocean cluster resides
583 predominantly in the southern part of the Arctic and the permanent sea-ice cluster in
584 the central Arctic. These two clusters have no or weak seasonal changes (constant
585 zero for open-ocean clusters and variation between 100% and 70% SIC for
586 permanent sea-ice). To better shape our understanding of seasonal cycles which
587 strongly change (from no ice to 70% SIC for the partial winter-freezing clusters and to
588 100% SIC for the full winter-freezing cluster), we distinguish which areas are mainly
589 associated with each of these two clusters by plotting the difference of probability
590 between these two clusters for the whole period (Figure 9). It displays spatially
591 consistent regions. The inner belt connecting the Baffin Bay to northern Barents is
592 attached to the coastal Arctic and is dominated by the full winter freezing cluster.
593 Further south, this cluster is surrounded by an outer belt from the southern Barents
594 to the southern Labrador Sea and by the Bering Sea dominated by the partial
595 winter-freezing cluster. Thus, the full winter-freezing cluster is more likely to occur in
596 coastal areas than the partial winter-freezing cluster. This spatial repartition might be
597 explained by the difference in year-round shapes of the seasonal cycles:
598 quasi-sinusoidal for partial winter-freezing and asymmetric for full winter-freezing.
599 Indeed, Eisenman (2010) demonstrates that the coastlines, by blocking the sea-ice
600 growth, drive the asymmetric seasonal cycle's shape while sea-ice free to grow and
601 melt (not being blocked by land) has a sinusoidal shape. Our results corroborate this
602 finding.

603

604

605



606

607 Figure 9: Map of the probability of the full winter-freezing cluster minus the partial
 608 winter-freezing cluster averaged over the period 1979-2023. The dotted thin and
 609 thick lines are the mean SIC of 0.15 and 0.8 for the period 1979-2023, respectively.

610

611 3.3 Regime stability and transition

612 In order to describe the grid-cell evolution of the Arctic sea ice over the period
613 1979-2023, we further classify each grid cell into four regimes: stable, unstable,
614 destabilization, and stabilization. First, we define a stable phase as a sequence when
615 the cluster having the maximum probability stays the same for at least 10 years in a
616 row, allowing for a tolerance of 1 year to belong to a different cluster within that
617 period. Sensitivity tests have been performed on this definition (Figure S3), and the
618 results do not change when we apply small definition changes (i.e., 9 to 11 years
619 minimum length of the same cluster with zero to 2 years of tolerance). Second, we
620 label each grid cell as follows:

- 621 1. Grid cells being in a unique stable phase over the whole period
622 (1979-2023) are labelled stable regime;
- 623 2. Grid cells belonging to a stable phase at the end of the period and not
624 being in a stable phase before or being in another stable phase (with a
625 different dominant cluster) before are labelled stabilization;
- 626 3. Grid cells not being in a stable phase at the end of the period and being
627 in a stable phase before are labelled destabilization;
- 628 4. Grid cells not being in a stable phase during the whole period or one or
629 several stable phases between periods of not stable phases are labelled
630 unstable.

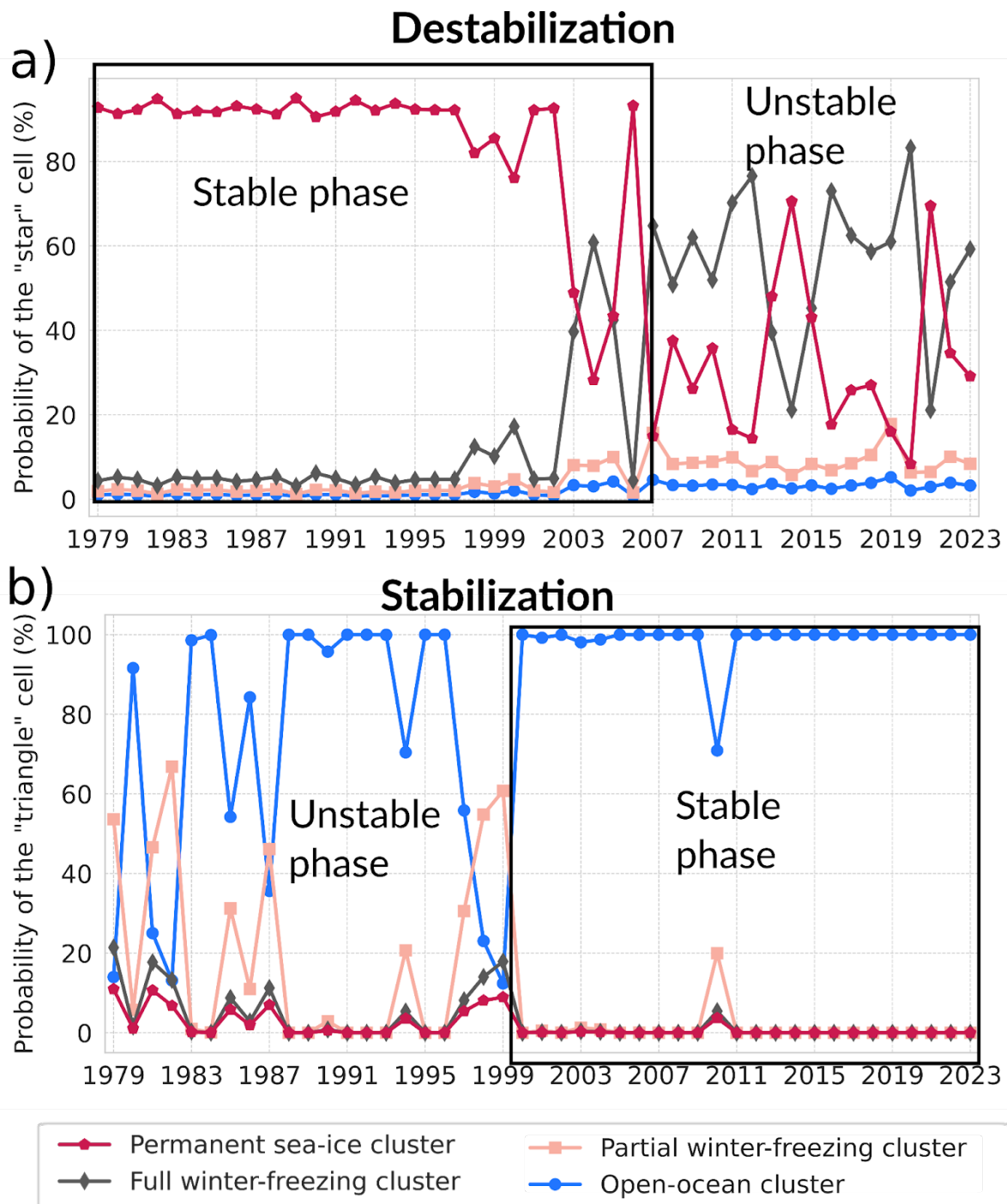
631 Figure 10 illustrates how we define the stabilization and destabilization labels.

632

633

634

635



636

637 Figure 10: Evolution of clusters at the location denoted by the star (a) and the triangle
 638 (b) in Figure 11. The stable phase is delimited by a black rectangle. These locations
 639 have been chosen to illustrate the destabilization and stabilization label of the Arctic
 640 sea ice evolution, respectively.

641

As shown in Figure 11, the stable region predominantly covers the central part of the Arctic Ocean, including the area around the North Pole, following most of the regions covered by permanent sea-ice cluster, as well as the ocean regions in the open-ocean cluster. Smaller regions present stable conditions: the northern Baffin Bay and southeast of Kara Sea dominated by the full winter-freezing cluster and northern Bering Sea associated with the partial winter-freezing cluster (Figure 8). Some regions jump between two or more clusters during the whole period, experiencing an unstable regime. These regions are sparse, the biggest being the northern Barents and Kara Seas. Most unstable regime areas are sitting in between stabilization and destabilization regimes areas.

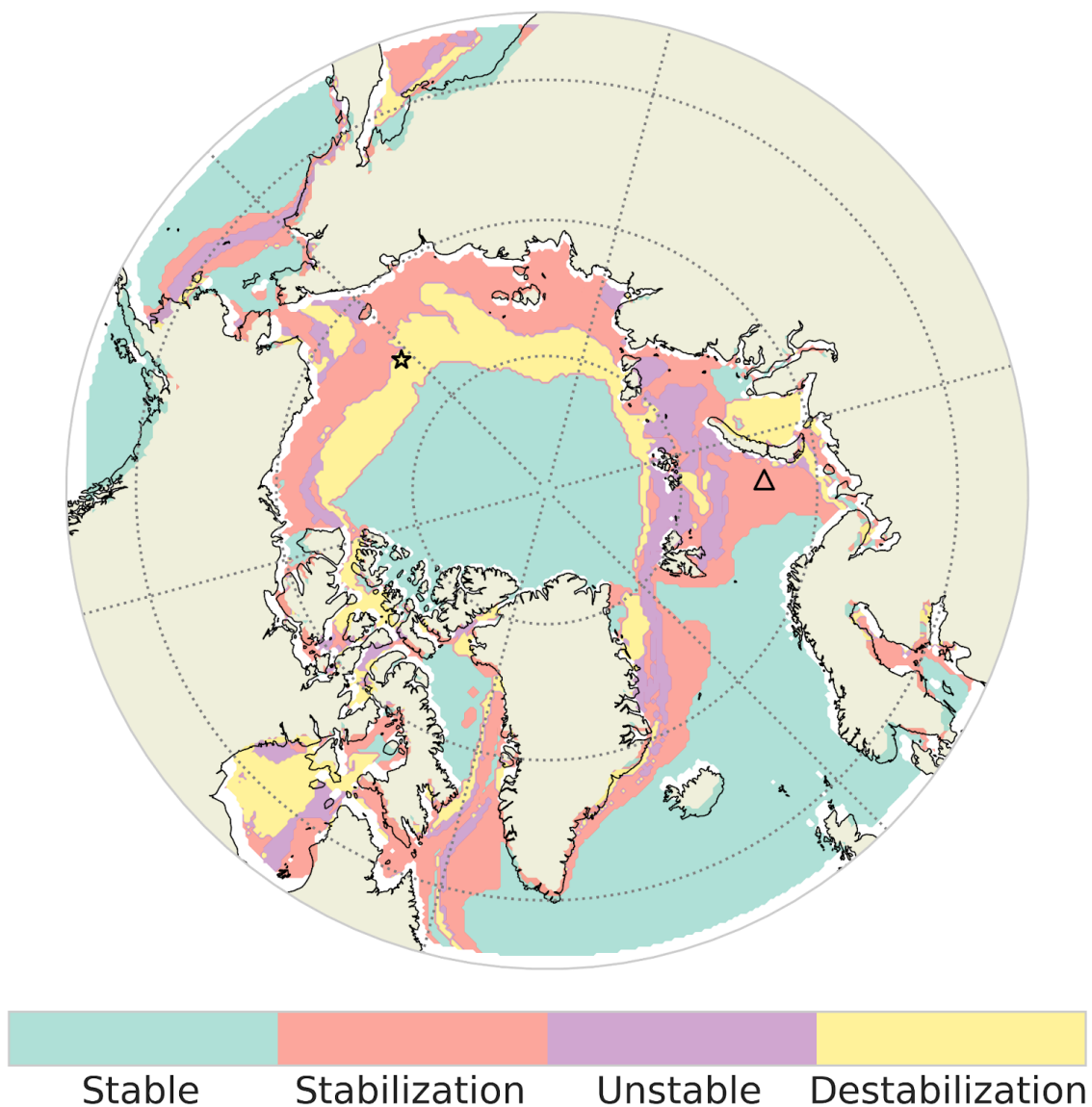


Figure 11: Map of the four regimes (stable, stabilization, unstable, and destabilization) used to describe the evolution of Arctic clusters based on sea-ice seasonal cycles. The star and triangle markers indicated the two localizations used to illustrate the destabilization and stabilization in Figure 10 respectively.

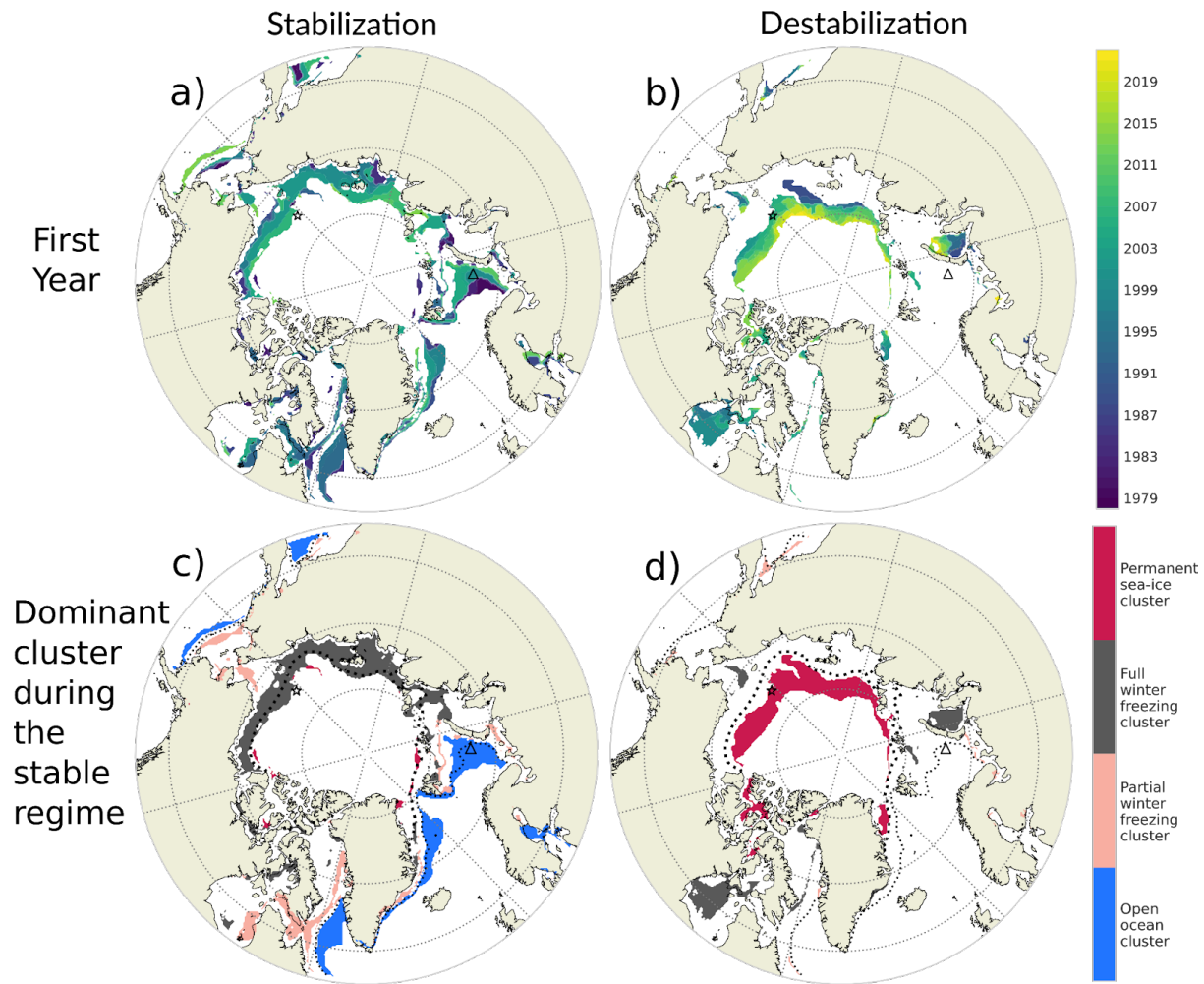
To describe the stabilization and destabilization regimes, we display the dominant cluster (the cluster having the maximum probability) during the stable phase of these two regimes (early period for the destabilization regime and late period for the stabilization period; Figure 12c and 12d). And, to quantify the year of transition, we introduce the year of stabilization as the first year when the stable phase occurs until the end of the whole period (Fig. 12a), and the year of destabilization as the last year of the stable phase (Fig. 12b). One should note that according to our definition the maximum year of stabilization is 2013 and minimum year of destabilization is 1989.

An inner belt shape (from southern Beaufort Sea to the southern Kara) connecting parts of the Barents Sea and around Greenland (Greenland Sea and Labrador Sea) is labeled stabilization (Figure 11). The inner belt shape stabilized to the full winter-freezing cluster while the other regions in the Atlantic side (Barents to Labrador Sea) stabilized to the open-ocean cluster (Figure 12c). This is in link with the shift of the permanent sea-ice cluster to the full winter freezing cluster in the Pacific side and the expansion of the open-ocean cluster in the Atlantic side (Figure 8). This transition occurred in a northward propagation starting in the 80's in the Barents Sea for the Atlantic side and in the Laptev in for the Pacific side (Figure 12a).

The belt from the northern Canadian Archipelago to the northern Greenland Sea (wider from the Beaufort Sea to Laptev Sea) is in the destabilization regime. These regions lost their typical permanent sea-ice cluster (Figure 12d) being mainly replaced by the full winter freezing cluster (Figure 8) in a northward propagation. The southeast Kara Sea and Hudson Bay, in a northward propagation for the former and during the 2000's for the Hudson Bay (Figure 12b).

683 In summary, the four regimes illustrate how different regions of the Arctic have
 684 experienced changes in stability. This regionalization suggests a more latitudinal
 685 vision of the region, as for the Seas from the Beaufort to the Kara Seas, the southern
 686 parts is experiencing a stabilization to a new cluster and the northern part a
 687 destabilization of an old cluster.

688



689

690 Figure 12: First year of stabilization (a) and destabilization (b) and associated
 691 dominant cluster for the stable regime of the stabilization (c) and destabilization (d).
 692 The star and triangle markers indicated the two localizations used to illustrate the
 693 destabilization and stabilization in Figure 10, respectively.

4. Conclusion and Discussion

This paper explores the use of a data-driven method using satellite observation of SIC to study the spatio-temporal evolution of sea ice in the Arctic over the period 1979-2023. We determine Arctic regions based on statistically different sea-ice seasonal cycles, and describe Arctic changes through the time evolving borders. The methodology is based on the clustering (machine learning method) of the full sea-ice seasonal cycle, instead of classic descriptors used in previous studies (e.g., sea-ice extent, sea-ice age and ice-free duration). It shows that the Arctic sea ice changes are best described with four clusters of seasonal cycles: the open-ocean cluster (with no ice during the whole year), the permanent sea-ice cluster (total sea-ice coverage with a minimum of 70% SIC in September), and two clusters showing ice-free conditions in late summer, namely the partial winter-freezing cluster and the full winter-freezing cluster. The full winter-freezing cluster has a larger SIC in winter, displays a more abrupt summer melting and winter freezing and has a shorter ice-free season than the partial winter-freezing one. The central Arctic belongs to the permanent sea-ice cluster. According to this clustering, a first date of retreat in early July has around 70% of chance to belong to the full winter-freezing cluster which shows ice-free conditions in summer. A first date of advance in early September has around 95% of chance to belong to the full winter freezing cluster which presents fully ice covered condition in the following winter.

Another important aspect of our analysis is that a given seasonal cycle can be in between two or more seasonal cycle centroids. We therefore believe that a probabilistic view when dealing with clustering is important. By analysis the evolution of the pan-Arctic clusterings over the 1979-2023 period, we show that the probability to belong to the permanent sea-ice seasonal cycle has decreased by 3.1 %/decade which is compensated with an increase of probability to belong to the open-ocean cluster (1.6 % per decade), the full winter freezing cluster (1.1 % per decade) and to a smaller extent to the partial winter-freezing cluster (0.5 % per decade). Regional shift in the clusters occurs over time. In general, the permanent sea-ice retraction from the Pacific side is compensated by the full winter-freezing

724 cluster and the open-ocean cluster expansion in the Atlantic side is compensated by
725 loss of the partial winter-freezing cluster.

726 We introduce another diagnostic to quantify the regime stability and transition
727 of the Arctic sea ice. The stable region (having always the same dominant cluster for
728 the whole period 1979-2023) predominantly covers the central part of the Arctic
729 Ocean, including the area around the North Pole, following most of the regions
730 covered by permanent sea-ice cluster, as well as the ocean regions in the open-ocean
731 cluster. Smaller regions present stable conditions: the northern Baffin Bay and
732 southeast of Kara Sea dominated by the full winter-freezing cluster and northern
733 Bering Sea associated with the partial winter-freezing cluster. From the Beaufort to
734 the Kara Seas, the southern parts have stabilized (experiencing a new typical seasonal
735 cycle, corresponding to the full winter-freezing cluster) and the northern part have
736 destabilized (losing their typical permanent sea-ice seasonal cycle).

737 This regionalization suggests a more latitudinal vision of the region. Also, this
738 study calls for pan-Arctic sea-ice thickness observation in order to better understand
739 sea-ice changes.

740 5. Discussion

741 The k-means clustering of the sea-ice seasonal cycle we applied to the Arctic
742 shares similarities with the analysis of Wachter et al. (2021) for the Antarctic. The
743 main differences however reside in our use of Mahalanobis distances, to account for
744 the correlation between the months, and the initialization based on equal separation
745 of quantiles for the centroids, to avoid any random aspect in the clustering algorithm.
746 These two choices enable to constrain the clustering with physical features. Besides,
747 by the use of the Silhouette coefficient, we found the Arctic is best described with a
748 number of clusters of 3 (the open-ocean has been added afterward). This number has
749 also been found by Fuckar et al., (2016) using a suite of indices (Krzanowski-Lai,
750 Calinski-Harabasz, Duda-Hart J index, Ratkowsky-Lance, Ball-Hall, point-biserial, gap
751 statistic, McClain-Rao, tau and scatter-distance index) onto detrended sea-ice
752 thickness of an ocean-sea ice general circulation model. In contrast with Fuckar et al.,
753 (2016) that calculated time series of occurrences of clusters based on the

resemblance of the pan-Arctic pattern, our probabilistic method defines a time series of probability of occurrence of each cluster at the grid cell scale. This enables us to study the spatial evolution of the cluster areas, and therefore define spatio-temporal regions that share a common feature (in our case sea-ice seasonal cycle).

Our clustering approach is complementary to diagnostics involving the dates of melting and freezing onsets, which have been used to quantify changes in the duration and shift of ice-free seasons at the pan or regional Arctic scales (Markus et al., 2009; Stammerjohn et al., 2012; Parkinson 2014; Johnson & Eicken, 2016; Stroeve et al., 2014; Lebrun et al., 2019). Instead, our method enables us to target regions experiencing a redistribution to another typical seasonal cycle representing longer and ice-free seasons, and retrieve the year of the shift. Another advantage is that we do not use any arbitrary cutoff of SIC. Additionally, our diagnostic delimits regions with the same sea-ice seasonal dynamics. The major drawback of our approach resides in the exact grid point quantification of the real seasonal cycle features (such as ice-free duration), as we gather grid cells within a type represented by a single seasonal cycle (the centroid). However, considering the full seasonal cycle gives useful information, as its derivative gives the period of melting and growth. Therefore, the two diagnostics complement each other nicely.

By doing the diagnostic of the trend in the length of the sea-ice season for the period 1979-2013, Parkinson (2014) shows that the length of the ice season has shortened in almost all the coastal regions (around -10 days/decade with a maximum -30 days/decade in the northern Chukchi Sea and around -50 days/decade in the northern Barents Sea), the main exceptions being the Bering Sea, portions of the Canadian Archipelago (around +10 days/decade) and the central Arctic where the sea-ice season duration remain unchanged over the period. Similar features are obtained in Lebrun et al., (2019) who considered the period up to 2015. Also, Lukovich and Barber (2007) examination of spatial coherence in SIC anomalies indicates that maximum SIC anomalies prevail near the Kara Sea, Beaufort Sea, and Chukchi Sea regions during late summer/early fall from 1979 to 2004. All these studies are consistent with our results showing a decrease in probability for the

785 permanent sea-ice cluster of about 3.1% per decade, especially in coastal regions of
786 the Pacific side of the Arctic, leading to a shortening of the seasonal cycle. Moreover,
787 we were able to show that this regime transition occurs in a smooth northward
788 propagation.

789 Our clustering approach suggests that the first date of freezing and advance
790 could be key for predicting ice conditions around 6 months in advance. This feature
791 follows a physical behaviour of sea-ice shown by Stammerjohn (2012) and Stroeve et
792 al. (2016). They found strong correlations between the dates of the spring sea-ice
793 retreat and subsequent autumn sea-ice advance (i.e., over the summer), indicating
794 that an early sea-ice retreat is often followed by a late autumn sea-ice advance and
795 conversely, a late sea-ice retreat is often followed by an early autumn sea-ice
796 advance. Indeed, consistent with our clustering analysis, the partial winter-freezing
797 cluster has an early sea-ice retreat (in March) and late autumn sea-ice advance
798 (mid-October) while the full winter-freezing cluster has a late sea-ice retreat (in April)
799 and early autumn sea-ice advance (mid-September). Therefore, this simple model
800 suggests that the first date of retreat could be a good indicator for ice-free conditions
801 the following summer and the first date of advance a good indicator for fully ice
802 cover conditions the following winter. A redefined model which quantifies this
803 without taking into accounts specified clustering is out of the scope of the study. An
804 example of such studies has been done in the Antarctic and shows that at interannual
805 timescales, retreat date anomalies are constrained by seasonal maximum ice
806 thickness (Himminch et al., 2025) and the advance date is controlled by the timing of
807 sea-ice retreat through heat stored in the summer ocean mixed layer (Himmich et al.,
808 2023). In the Arctic, Gregory et al., 2020 by setting up a complex network statistical
809 approach, shows good predictive skills for regional September SIE from previous June
810 SIC, especially toward the Pacific sector.

811 Concerning the growth and melting of sea-ice, Parkinson et al., 1999 and
812 Parkinson and Cavalieri, 2008 showed that the seasonal decay of sea ice extent is
813 gradual during early summer and then accelerates during the remaining summer
814 months, whereas wintertime growth is most rapid in early winter. A standard
815 explanation suggests that this asymmetry between seasonal growth and decay is
816 caused by rapid temperature changes driven by air masses from the Eurasian

continent (Peixoto and Oort, 1992). Here this asymmetry in the seasonal cycle is seen only for the permanent sea-ice cluster and full winter freezing cluster, suggesting that the partial winter sea-ice is driven by another driver. The full winter-freezing cluster (with no sinusoidal feature) is more likely present along the Arctic coastline than the partial winter-freezing cluster (with a sinusoidal feature). The reason for this spatial repartition could be explained by the fact that the sinusoidal feature of the sea-ice seasonal cycle is linked to the ability of the ice to freeze and expand freely, without being blocked by land, as suggested by Eisenman (2010).

A limitation of the study is the fact that the method accounts solely for the area between the centroid and the seasonal cycles to define the clusters, meaning that there is no constraint to have the same maximum and minimum to belong to one cluster. However, if the shift of minimum or maximum is large, the area will largely increase which prevents having a large discrepancy between the maximum and minimum of the seasonal cycles and their respective centroids. Another limitation of this study is that sea-ice dynamics are analysed using SIC rather than sea-ice volume (which would better represent sea-ice behaviour, including growth and melting), due to the lack of robust and long-term sea-ice thickness data.

The introduction in this paper of the clustering of the Arctic sea-ice seasonal cycle, with its statistical aspect, can provide an approach to validate the dynamics of sea-ice in climate models. Indeed, applying the clustering method described here to models could inform if a given model has the same number of optimal clusters and the types of seasonal cycles as the one obtained from observations. It could also be used to answer how different clusters will be distributed for different future scenarios. Overall, this methodology is transposable to other variables to better answer its past and future variability in a robust statistical framework.

Author's contribution

All authors contributed to the conceptual design of the study and the interpretation of the results. AS, PT, and FS established the methodological framework. AS developed the code, generated the figures, and drafted the initial version of the article. PT, FS, and CL carefully revised the paper contributing to its improvement.

848

849 *Financial support*

850 This study is funded by ANR and France 2030 through the project CLIMArcTIC (grant
851 ANR-22-POCE-0005)

852

853 *Competing interests*

854 The contact author has declared that none of the authors has any competing
855 interests.

856

857 *Code and data availability*

858 The daily SIC satellite data from the National Snow and Ice Data Center (NSIDC) are
859 openly available and can be found at <https://doi.org/10.7265/efmz-2t65> (Meier et al.,
860 2021)

861

862 *Acknowledgement*

863 We enthusiastically thank the three reviewers for their very constructive comments
864 that helped to improve the paper.

865

866 We acknowledge the use of Mistral (<https://chat.mistral.ai/chat>) and ChatGPT
867 (<https://chat.openai.com/>) to generate some materials (code) that we have adapted to
868 include in this study.

869

870 For the purpose of Open Access, a CC-BY public copyright licence has been applied
871 by the authors to the present document and will be applied to all subsequent
872 versions up to the Author Accepted Manuscript arising from this submission

873

874 *References*

875 Aksenov, Y., Popova, E. E., Yool, A., Nurser, A. G., Williams, T. D., Bertino, L., & Bergh,
876 J. (2017). On the future navigability of Arctic sea routes: High-resolution projections
877 of the Arctic Ocean and sea ice. *Marine Policy*, 75, 300-317.

878

879 Ardyna, M., & Arrigo, K. R. (2020). Phytoplankton dynamics in a changing Arctic
880 Ocean. *Nature Climate Change*, 10(10), 892-903.

881

882 Bushuk, M., Ali, S., Bailey, D. A., Bao, Q., Batté, L., Bhatt, U. S., ... & Zhang, Y. (2024).
883 Predicting September Arctic Sea Ice: A Multi-Model Seasonal Skill Comparison.
884 *Bulletin of the American Meteorological Society*.

885

886 Cavalieri, D. J., Gloersen, P., & Campbell, W. J. (1984). Determination of sea ice
887 parameters with the Nimbus 7 SMMR. *Journal of Geophysical Research*:

888 Atmospheres, 89(D4), 5355-5369.

889

890 Cocetta, F., Zampieri, L., Selivanova, J., & Iovino, D. (2024). Assessing the
891 representation of Arctic sea ice and the marginal ice zone in ocean–sea ice
892 reanalyses. *The Cryosphere*, 18(10), 4687-4702.

893

894 Cohen, J., Zhang, X., Francis, J., Jung, T., Kwok, R., Overland, J., Ballinger, T. J., Bhatt,
895 U. S., Chen, H. W., Coumou, D., Feldstein, S., Gu, H., Handorf, D., Henderson, G.,
896 Ionita, M., Kretschmer, M., Laliberte, F., Lee, S., Linderholm, H. W., and Yoon, J.:
897 Divergent consensus on Arctic amplification influence on mid-latitude severe winter
898 weather, *Nat. Clim. Change*, 10, 20–29, <https://doi.org/10.1038/s41558-019-0662-y>,
899 2020

900

901 Comiso, J. C. (1986). Characteristics of Arctic winter sea ice from satellite
902 multispectral microwave observations. *Journal of Geophysical Research: Oceans*,
903 91(C1), 975-994.

904

905 Delhaye, S., Massonnet, F., Fichet, T., Msadek, R., Terray, L., & Screen, J. (2024).
906 Dominant role of early winter Barents–Kara sea ice extent anomalies in subsequent
907 atmospheric circulation changes in CMIP6 models. *Climate Dynamics*, 62(4),
908 2755-2778.

909

910 Deser, C., Tomas, R. A., and Sun, L. (2015). The role of ocean–atmosphere coupling in
911 the zonal-mean atmospheric response to Arctic sea-ice loss, *J. Climate*, 28,
912 2168–2186.

913

914 Eisenman, I. (2010). Geographic muting of changes in the Arctic sea ice cover.
915 *Geophysical Research Letters*, 37(16).

916

917 Eyring, V., N.P. Gillett, K.M. Achuta Rao, R. Barimalala, M. Barreiro Parrillo, N.
918 Bellouin, C. Cassou, P.J. Durack, Y. Kosaka, S. McGregor, S. Min, O. Morgenstern, and
919 Y. Sun, 2021: Human Influence on the Climate System. In *Climate Change 2021: The*
920 *Physical Science Basis. Contribution of Working Group I to the Sixth Assessment*
921 *Report of the Intergovernmental Panel on Climate Change* [Masson-Delmotte, V., P.
922 Zhai, A. Pirani, S.L. Connors, C. Péan, S. Berger, N. Caud, Y. Chen, L. Goldfarb, M.I.
923 Gomis, M. Huang, K. Leitzell, E. Lonnoy, J.B.R. Matthews, T.K. Maycock, T. Waterfield,
924 O. Yelekçi, R. Yu, and B. Zhou (eds.)]. Cambridge University Press, Cambridge, United
925 Kingdom and New York, NY, USA, pp. 423–552, doi:10.1017/9781009157896.005.

926

927 Forster, P., T. Storelvmo, K. Armour, W. Collins, J.-L. Dufresne, D. Frame, D.J. Lunt, T.
928 Mauritsen, M.D. Palmer, M. Watanabe, M. Wild, and H. Zhang, 2021: The Earth's
929 Energy Budget, Climate Feedbacks, and Climate Sensitivity. In *Climate Change 2021:*
930 *The Physical Science Basis. Contribution of Working Group I to the Sixth Assessment*
931 *Report of the Intergovernmental Panel on Climate Change* [Masson-Delmotte, V., P.
932 Zhai, A. Pirani, S.L. Connors, C. Péan, S. Berger, N. Caud, Y. Chen, L. Goldfarb, M.I.
933 Gomis, M. Huang, K. Leitzell, E. Lonnoy, J.B.R. Matthews, T.K. Maycock, T. Waterfield,
934 O. Yelekçi, R. Yu, and B. Zhou (eds.)]. Cambridge University Press, Cambridge, United
935 Kingdom and New York, NY, USA, pp. 923–1054, doi:10.1017/9781009157896.009.

936

937 Fox-Kemper, B., H.T. Hewitt, C. Xiao, G. Aðalgeirsdóttir, S.S. Drijfhout, T.L. Edwards,
938 N.R. Golledge, M. Hemer, R.E. Kopp, G. Krinner, A. Mix, D. Notz, S. Nowicki, I.S.
939 Nurhati, L. Ruiz, J.-B. Sallée, A.B.A. Slangen, and Y. Yu, 2021: Ocean, Cryosphere and
940 Sea Level Change. In *Climate Change 2021: The Physical Science Basis. Contribution*
941 *of Working Group I to the Sixth Assessment Report of the Intergovernmental Panel*
942 *on Climate Change* [Masson-Delmotte, V., P. Zhai, A. Pirani, S.L. Connors, C. Péan, S.
943 Berger, N. Caud, Y. Chen, L. Goldfarb, M.I. Gomis, M. Huang, K. Leitzell, E. Lonnoy,
944 J.B.R. Matthews, T.K. Maycock, T. Waterfield, O. Yelekçi, R. Yu, and B. Zhou (eds.)].
945 Cambridge University Press, Cambridge, United Kingdom and New York, NY, USA, pp.
946 1211–1362, doi:10.1017/9781009157896.011.

947

948 Fučkar, N. S., Guemas, V., Johnson, N. C., Massonnet, F., & Doblas-Reyes, F. J. (2016).
949 Clusters of interannual sea ice variability in the northern hemisphere. *Climate*
950 *Dynamics*, 47(5), 1527–1543. <https://doi.org/10.1007/s00382-015-2917-2>

951

952 Galley, R. J., Else, B. G. T., Prinsenberg, S. J., Babb, D., & Barber, D. G. (2013). Summer
953 sea ice concentration, motion, and thickness near areas of proposed offshore oil and
954 gas development in the Canadian Beaufort Sea—2009. *Arctic*, 105–116.

955

956 GEBCO Compilation Group. (2024). GEBCO 2024 Grid.
957 doi:10.5285/1c44ce99-0a0d-5f4f-e063-7086abc0ea0f . Date Accessed: 6 Feb. 2025

958

959 Goosse, H., Kay, J. E., Armour, K. C., Bodas-Salcedo, A., Chepfer, H., Docquier, D., ... &
960 Vancoppenolle, M. (2018). Quantifying climate feedbacks in polar regions. *Nature*
961 *communications*, 9(1), 1919.

962

963 Gregory, W., Tsamados, M., Stroeve, J., & Sollich, P. (2020). Regional September sea
964 ice forecasting with complex networks and Gaussian processes. *Weather and*
965 *Forecasting*, 35(3), 793–806.

966

967 Gregory, W., Stroeve, J., & Tsamados, M. (2022). Network connectivity between the
968 winter Arctic Oscillation and summer sea ice in CMIP6 models and observations. *The*
969 *Cryosphere*, 16(5), 1653–1

970

971 Gulev, S.K., P.W. Thorne, J. Ahn, F.J. Dentener, C.M. Domingues, S. Gerland, D. Gong,
972 D.S. Kaufman, H.C. Nnamchi, J. Quaas, J.A. Rivera, S. Sathyendranath, S.L. Smith, B.
973 Trewin, K. von Schuckmann, and R.S. Vose, 2021: Changing State of the Climate
974 System. In *Climate Change 2021: The Physical Science Basis. Contribution of*
975 *Working Group I to the Sixth Assessment Report of the Intergovernmental Panel on*
976 *Climate Change* [Masson-Delmotte, V., P. Zhai, A. Pirani, S.L. Connors, C. Péan, S.
977 Berger, N. Caud, Y. Chen, L. Goldfarb, M.I. Gomis, M. Huang, K. Leitzell, E. Lonnoy,
978 J.B.R. Matthews, T.K. Maycock, T. Waterfield, O. Yelekçi, R. Yu, and B. Zhou (eds.)].
979 Cambridge University Press, Cambridge, United Kingdom and New York, NY, USA, pp.
980 287–422, doi:10.1017/9781009157896.004.

981

982 Himmich, K., Vancoppenolle, M., Madec, G., Sallée, J. B., Holland, P. R., & Lebrun, M.
983 (2023). Drivers of Antarctic sea ice advance. *Nature Communications*, 14(1), 6219.

984
985 Himmich, K., Vancoppenolle, M., Stammerjohn, S., Bocquet, M., Madec, G., & Fleury,
986 S. (2025). Local drivers of Antarctic spring sea ice retreat. *Geophysical Research Letters*,
987 52(10), e2025GL114764.
988
989 Huntington, H. P., Quakenbush, L. T. & Nelson, M. (2017). Evaluating the effects of
990 climate change on indigenous marine mammal hunting in northern and western
991 alaska using traditional knowledge. *Front. Mar. Sci.* 4, 319
992
993 Houghton, I. A., & Wilson, J. D. (2020). El Niño detection via unsupervised clustering
994 of Argo temperature profiles. *Journal of Geophysical Research: Oceans*, 125,
995 e2019JC015947. <https://doi.org/10.1029/2019JC015947>
996
997 Huntington, H. P., Danielson, S. L., Wiese, F. K., Baker, M., Boveng, P., Citta, J. J., ... &
998 Wilson, C. (2020). Evidence suggests potential transformation of the Pacific Arctic
999 ecosystem is underway. *Nature Climate Change*, 10(4), 342-348.
1000
1001 IPCC, 2019: Summary for Policymakers. In: IPCC Special Report on the Ocean and
1002 Cryosphere in a Changing Climate [H.-O. Pörtner, D.C. Roberts, V. Masson-Delmotte,
1003 P. Zhai, M. Tignor, E. Poloczanska, K. Mintenbeck, A. Alegría, M. Nicolai, A. Okem, J.
1004 Petzold, B. Rama, N.M. Weyer (eds.)]. Cambridge University Press, Cambridge, UK
1005 and New York, NY, USA, pp. 3–35. <https://doi.org/10.1017/9781009157964.001>.
1006
1007 IPCC, 2021: Summary for Policymakers. In: *Climate Change 2021: The Physical*
1008 *Science Basis. Contribution of Working Group I*
1009 *to the Sixth Assessment Report of the Intergovernmental Panel on Climate Change*
1010 [Masson-Delmotte, V., P. Zhai, A. Pirani, S.L.
1011 Connors, C. Péan, S. Berger, N. Caud, Y. Chen, L. Goldfarb, M.I. Gomis, M. Huang, K.
1012 Leitzell, E. Lonnoy, J.B.R. Matthews, T.K.
1013 Maycock, T. Waterfield, O. Yelekçi, R. Yu, and B. Zhou (eds.)]. Cambridge University
1014 Press, Cambridge, United Kingdom and New
1015 York, NY, USA, pp. 3–32, doi:10.1017/9781009157896.001.
1016
1017 Jain, A. K. (2010). Data clustering: 50 years beyond K-means. *Pattern recognition*
1018 *letters*, 31(8), 651-666.
1019
1020 Jambudi T, Gandhi S (2022) An Effective Initialization Method Based on Quartiles for
1021 the K-means Algorithm. *Indian Journal of Science and Technology* 15(35):
1022 1712-1721.
1023 <https://doi.org/10.17485/IJST/v15i35.714>
1024
1025 Johannessen, O. M., Kuzmina, S. I., Bobylev, L. P., & Miles, M. W. (2016). Surface air
1026 temperature variability and trends in the Arctic: new amplification assessment and
1027 regionalisation. *Tellus A: Dynamic Meteorology and Oceanography*, 68(1), 28234.
1028
1029 Johnson, M., & Eicken, H. (2016). Estimating Arctic sea-ice freeze-up and break-up
1030 from the satellite record: A comparison of different approaches in the Chukchi and
1031 Beaufort Seas. *Elementa*, 4, 000124.

1032
1033 Kwok, R. (2007). Near zero replenishment of the Arctic multiyear sea ice cover at the
1034 end of 2005 summer. *Geophysical Research Letters*, 34(5).
1035
1036 Lebrun, M., Vancoppenolle, M., Madec, G., & Massonnet, F. (2019). Arctic sea-ice-free
1037 season projected to extend into autumn. *The Cryosphere*, 13(1), 79-96.
1038
1039 Lee, J.-Y., J. Marotzke, G. Bala, L. Cao, S. Corti, J.P. Dunne, F. Engelbrecht, E. Fischer,
1040 J.C. Fyfe, C. Jones, A. Maycock, J. Mutemi, O. Ndiaye, S. Panickal, and T. Zhou, 2021:
1041 Future Global Climate: Scenario-Based Projections and Near-Term Information. In
1042 Climate Change 2021: The Physical Science Basis. Contribution of Working Group I
1043 to the Sixth Assessment Report of the Intergovernmental Panel on Climate Change
1044 [Masson-Delmotte, V., P. Zhai, A. Pirani, S.L. Connors, C. Péan, S. Berger, N. Caud, Y.
1045 Chen, L. Goldfarb, M.I. Gomis, M. Huang, K. Leitzell, E. Lonnoy, J.B.R. Matthews, T.K.
1046 Maycock, T. Waterfield, O. Yelekçi, R. Yu, and B. Zhou (eds.)]. Cambridge University
1047 Press, Cambridge, United Kingdom and New York, NY, USA, pp. 553–672,
1048 doi:10.1017/9781009157896.006.
1049
1050 Levine, X. J., Cvijanovic, I., Ortega, P., Donat, M. G., & Tourigny, E. (2021).
1051 Atmospheric feedback explains disparate climate response to regional Arctic sea-ice
1052 loss. *npj Climate and Atmospheric Science*, 4(1), 28.
1053
1054 Lukovich, J. V., & Barber, D. G. (2007). On the spatiotemporal behavior of sea ice
1055 concentration anomalies in the Northern Hemisphere. *Journal of Geophysical*
1056 *Research: Atmospheres*, 112(D13). <https://doi.org/10.1029/2006JD007836>
1057
1058 Markus, T., J. C. Stroeve, and J. Miller (2009), Recent changes in Arctic sea ice melt
1059 onset, freezeup, and melt season length, *J. Geophys. Res.*, 114, C12024,
1060 doi:10.1029/2009JC005436.
1061
1062 Maze, G., Mercier, H., Fablet, R., Tandeo, P., Radcenco, M. L., Lenca, P., ... & Le Goff, C.
1063 (2017). Coherent heat patterns revealed by unsupervised classification of Argo
1064 temperature profiles in the North Atlantic Ocean. *Progress in Oceanography*, 151,
1065 275-292.
1066
1067 Meier, W. N., Stroeve, J., & Fetterer, F. (2007). Whither Arctic sea ice? A clear signal of
1068 decline regionally, seasonally and extending beyond the satellite record. *Annals of*
1069 *Glaciology*, 46, 428-434.
1070
1071 Mao, J., & Jain, A. K. (1996). A self-organizing network for hyperellipsoidal clustering
1072 (HEC). *IEEE transactions on neural networks*, 7(1), 16-29.
1073
1074 Maslanik, J., J. Stroeve, C. Fowler, and W. Emery (2011), Distribution and trends in
1075 Arctic sea ice age through spring 2011, *Geophys. Res. Lett.*, 38, L13502,
1076 doi:10.1029/2011GL047735.
1077
1078 Meier, W. N., F. Fetterer, A. K. Windnagel, and J. S. Stewart. (2021). NOAA/NSIDC

Climate Data Record of Passive Microwave Sea Ice Concentration, Version 4 [Data Set]. Boulder, Colorado USA. National Snow and Ice Data Center.
<https://doi.org/10.7265/efmz-2t65>. Date Accessed 15-07-2024.

Meier, W. N., Stewart, J. S., Windnagel, A., & Fetterer, F. M. (2022). Comparison of hemispheric and regional sea ice extent and area trends from NOAA and NASA passive microwave-derived climate records. *Remote Sensing*, 14(3), 619.

Meier, W. N., & Stroeve, J. (2022). An updated assessment of the changing Arctic sea ice cover. *Oceanography*, 35(3/4), 10-19.

Meier, Walter N., and J. Scott Stewart. (2023). NSIDC Land, Ocean, Coast, Ice, and Sea Ice Region Masks. NSIDC Special Report 25. Boulder CO, USA: National Snow and Ice Data Center.
<https://nsidc.org/sites/default/files/documents/technical-reference/nsidc-special-report-25.pdf>

Parkinson, C.L., J.C. Comiso, H.J. Zwally, D.J. Cavalieri, P. Gloersen, and W.J. Campbell, (1987). Arctic sea ice, 1973-1976: Satellite passive-microwave observations, NASA Special Publication, SP-489, 296 pp.,
<https://ntrs.nasa.gov/citations/19870015437>.

Parkinson, C.L., D.J. Cavalieri, P. Gloersen, H.J. Zwally, and J.C. Comiso, (1999). Arctic sea ice extents, areas, and trends, 1978–1996, *J. Geophys. Res.*, 104(C9), 20837–20856, <https://doi.org/10.1029/1999JC900082>.

Parkinson, C. L., & Cavalieri, D. J. (2008). Arctic sea ice variability and trends, 1979–2006. *Journal of Geophysical Research: Oceans*, 113(C7).

Parkinson, C. L. (2014), Spatially mapped reductions in the length of the Arctic sea ice season, *Geophys. Res. Lett.*, 41, 4316–4322, doi:10.1002/2014GL060434

Parkinson, C. L., and J. C. Comiso (2013), On the 2012 record low Arctic sea ice cover: Combined impact of preconditioning and an August storm, *Geophys. Res. Lett.*, 40, 1356–1361, doi:10.1002/grl.50349

Parkinson, C.L.; Comiso, J.C.; Zwally, H.J.; Cavalieri, D.J.; Gloersen, P.; Campbell, W.J. Arctic Sea Ice, 1973–1976: Satellite Passive-Microwave Observations; NASA SP-489; National Aeronautics and Space Administration: Washington, DC, USA, 1987; p. 296.

Peng, G., & Meier, W. N. (2018). Temporal and regional variability of Arctic sea-ice coverage from satellite data. *Annals of Glaciology*, 59(76pt2), 191-200.

Pedregosa, F., Michel, V., Grisel, O., Blondel, M., Prettenhofer, P., Weiss, R., et al. (2011). Scikit-learn: Machine learning in Python

Peng, G., & Meier, W. N. (2018). Temporal and regional variability of Arctic sea-ice coverage from satellite data. *Annals of Glaciology*, 59(76pt2), 191-200.

1127
 1128
 1129 Pithan, F., & Mauritsen, T. (2014). Arctic amplification dominated by temperature
 1130 feedbacks in contemporary climate models. *Nature geoscience*, 7(3), 181-184.
 1131
 1132 Petty, A. A., Stroeve, J. C., Holland, P. R., Boisvert, L. N., Bliss, A. C., Kimura, N., &
 1133 Meier, W. N. (2018). The Arctic sea ice cover of 2016: a year of record-low highs and
 1134 higher-than-expected lows. *The Cryosphere*, 12(2), 433-452.
 1135
 1136 Przybylak, R. (2002). Variability of air temperature and atmospheric precipitation in
 1137 the Arctic. Dordrecht, etc., Kluwer Academic Publishers
 1138
 1139 Przybylak, R. (2007). Recent air-temperature changes in the Arctic. *Annals of*
 1140 *Glaciology*, 46, 316-324.
 1141
 1142 Raphael, M. N., & Hobbs, W. (2014). The influence of the large-scale atmospheric
 1143 circulation on Antarctic sea ice during ice advance and retreat seasons:
 1144 RAPHAEL AND HOBBS; ANTARCTIC SEA ICE ADVANCE AND RETREAT.
 1145 *Geophysical Research Letters*, 41(14), 5037–5045.
 1146 <https://doi.org/10.1002/2014GL060365>
 1147
 1148 Regan, H. C., Rampal, P., Ólason, E., Boutin, G., & Korosov, A. (2022). Modelling the
 1149 evolution of Arctic multiyear sea ice over 2000–2018. *The Cryosphere Discussions*,
 1150 2022, 1-28.
 1151
 1152 Ricker, R., Hendricks, S., Kaleschke, L., Tian-Kunze, X., King, J., and Haas, C. , (2017). A
 1153 weekly Arctic sea-ice thickness data record from merged CryoSat-2 and SMOS
 1154 satellite data, *The Cryosphere*, 11, 1607–1623,
 1155 <https://doi.org/10.5194/tc-11-1607-2017>.
 1156
 1157 Rousseeuw, P. J. (1987). Silhouettes: a graphical aid to the interpretation and
 1158 validation of cluster analysis. *Journal of computational and applied mathematics*, 20,
 1159 53-65.
 1160
 1161 Shu, Q., Wang, Q., Årthun, M., Wang, S., Song, Z., Zhang, M., & Qiao, F. (2022). Arctic
 1162 Ocean Amplification in a warming climate in CMIP6 models. *Science advances*, 8(30),
 1163 eabn9755.
 1164
 1165 Siddon, E. C., Zador, S. G., & Hunt Jr, G. L. (2020). Ecological responses to climate
 1166 perturbations and minimal sea ice in the northern Bering Sea. *Deep Sea Research Part*
 1167 *II: Topical Studies in Oceanography*, 181, 104914.
 1168
 1169 Simon, A., Gastineau, G., Frankignoul, C., Rousset, C., and Codron, F. , (2021).
 1170 Transient climate response to Arctic sea-ice loss with two ice-constraining methods,
 1171 *J. Climate*, 34, 3295–3310, <https://doi.org/10.1175/JCLI-D-20-0288.1>.
 1172
 1173 Smith, L. C., & Stephenson, S. R. (2013). New Trans-Arctic shipping routes navigable
 1174 by midcentury. *Proceedings of the National Academy of Sciences*, 110(13),

1175 E1191-E1195.

1176

1177 Smith, D. M., Eade, R., Andrews, M. B., Ayres, H., Clark, A., Chripko, S., and Walsh, A.

1178 (2022) Robust but weak winter atmospheric circulation response to future Arctic

1179 sea-ice loss, *Nat. Commun.*, 13, 1–15.

1180

1181 Song, L., Zhao, X., Wu, Y., Gong, J., & Li, B. (2025). Assessing Arctic marginal ice zone

1182 dynamics from 1979 to 2023: insights into long-term variability and morphological

1183 changes. *Environmental Research Letters*, 20(3), 034032.

1184

1185 Stammerjohn, S., Massom, R., Rind, D., and Martinson, D.: Regions of rapid sea ice

1186 change (2012) An inter-hemispheric seasonal comparison, *Geophys. Res. Lett.*, 39,

1187 L06501, <https://doi.org/10.1029/2012GL050874>.

1188

1189 Stock, C. A. et al. (2017). Reconciling fisheries catch and ocean productivity. *Proc.*

1190 *Natl Acad. Sci. USA* 114, E1441–E1449.

1191

1192 Stroeve, J. C., T. Markus, L. Boisvert, J. Miller, and A. Barrett (2014), Changes in Arctic

1193 melt season and implications for sea ice loss, *Geophys. Res. Lett.*, 41, 1216–1225,

1194 doi:10.1002/2013GL058951.

1195

1196 Stroeve, J. C., Crawford, A. D., and Stammerjohn, S. (2016). Using timing of ice retreat

1197 to predict timing of fall freeze-up in the Arctic, *Geophys. Res. Lett.*, 43, GL069314,

1198 <https://doi.org/10.1002/2016GL069314>.

1199

1200 Sutherland, P., & Dumont, D. (2018). Marginal ice zone thickness and extent due to

1201 wave radiation stress. *Journal of Physical Oceanography*, 48(8), 1885–1901.

1202

1203

1204 Valko, I. (2014). Differentiating Arctic provinces: a cluster analysis of geographic and

1205 geopolitical indicators. *Central European Journal of International & Security Studies*,

1206 8(4).

1207

1208 Vancoppenolle, M., L. Bopp, G. Madec, J. Dunne, T. Ilyina, P. R. Halloran, and N.

1209 Steiner (2013), Future Arctic Ocean primary productivity from CMIP5 simulations:

1210 Uncertain outcome, but consistent mechanisms, *Global Biogeochem. Cycles*, 27,

1211 605–619, doi:10.1002/gbc.20055.

1212

1213 Wachter, P., Reiser, F., Friedl, P., & Jacobeit, J. (2021). A new approach to classification

1214 of 40 years of Antarctic sea ice concentration data. *International Journal of*

1215 *Climatology*, 41, E2683-E2699.

1216

1217

1218

1219

1220

1221